A theoretical individual-based model of Brown Ring Disease in Manila clams, Venerupis philippinarum

Christine Paillard, Fred Jean, Susan E. Ford, Eric N. Powell, John Klinck, Eileen E Hofmann, Jonathan Flye-Sainte-Marie

A theoretical individual-based model of Brown Ring Disease in Manila clams, *Venerupis philippinarum*

Christine Paillard [a,*], Fred Jean [a], Susan E. Ford [b], Eric N. Powell [b], John M. Klinck [c], Eileen E. Hofmann [c], Jonathan Flye-Sainte-Marie [a]

[a] *LEMAR UMR 6539, Institute Universitaire Européen de la Mer, Place Nicolas Copernic, 29280 Plouzané, France*
[b] *Haskin Shellfish Research Laboratory, Rutgers University, 6959 Miller Avenue, Port Norris, NJ 08349, USA*
[c] *Center for Coastal Physical Oceanography, Old Dominion University, Norfolk, VA 23508, USA*

An individual-based mathematical model was developed to investigate the biological and environmental inter-actions that influence the prevalence and intensity of Brown Ring Disease (BRD), a disease, caused by the bacte-rial pathogen, *Vibrio tapetis*, in the Manila clam (*Venerupis* (= *Tapes*, = *Ruditapes*) *philippinarum*). *V. tapetis* acts as an external microparasite, adhering at the surface of the mantle edge and its secretion, the periostracal lamina, causing the symptomatic brown deposit. Brown Ring Disease is atypical in that it leaves a shell scar that provides a unique tool for diagnosis of either live or dead clams. The model was formulated using laboratory and field mea-surements of BRD development in Manila clams, physiological responses of the clam to the pathogen, and the physiology of *V. tapetis*, as well as theoretical understanding of bacterial disease progression in marine shellfish. The simulation results obtained for an individual Manila clam were expanded to cohorts and populations using a probability distribution that prescribed a range of variability for parameters in a three dimensional framework; assimilation rate, clam hemocyte activity rate (the number of bacteria ingested per hemocyte per day), and clam calcification rate (a measure of the ability to recover by covering over the symptomatic brown ring deposit), which sensitivity studies indicated to be processes important in determining BRD prevalence and intensity. This approach allows concurrent simulation of individuals with a variety of different physiological capabilities (phenotypes) and hence by implication differing genotypic composition. Different combinations of the three variables provide robust estimates for the fate of individuals with particular characteristics in a population that consists of mixtures of all possible combinations.

The BRD model was implemented using environmental observations from sites in Brittany, France, where Manila clams routinely exhibit BRD signs. The simulated annual cycle of BRD prevalence and intensity agrees with observed disease cycles in cultured clam populations from this region, with maximum disease prevalence and in-tensity occurring from December to April. Sensitivity analyses of modeled physiological processes showed that the level of hemocyte activity is the primary intrinsic determinant of recovery of infected clams. Simulations de-signed to investigate environmental effects on BRD suggested that the outcome of the host–parasite interaction is dependent on food supply (high values being favorable for the host) and temperature. Results of simulations il-lustrate the complex interaction of temperature effects on propagation and viability of the bacterium, on the phagocytic activity of the hemocytes, and on other physiological processes of the host clam. Simulations using 1 °C and 2 °C increases in temperature generally favored disease development, indicating that climate warming might favor the spread of BRD.

1. Introduction

The mathematical models of disease epidemics described in the clas-sic papers of Kermack and McKendrick (1991a,b) (originally published in 1927 and reprinted in 1991) demonstrated the feasibility of using the-oretical frameworks to understand disease processes. From then until the late 1980s, disease modeling concentrated on mammalian popula-tions, including humans, with considerable interest also shown in para-sites and diseases of insects and plants (Anderson, 1982; Anderson and May, 1991; Bailey, 1975; Brown, 1987; Heesterbeek and Roberts, 1995; McCallum and Scott, 1994; Roberts et al., 1995). Since the late 1980s mathematical models were used to investigate host–parasite interac-tions in marine invertebrates (Blower and Roughgarden, 1987;

* Corresponding author at: LEMAR-UMR 6539, IUEM, Université de Bretagne Occidentale, Technopôle Brest Iroise, 29280 Plouzané, France. Tel.: +33 2 98 49 86 50; fax: +33 2 98 49 86 45.

E-mail address: christine.paillard@univ-brest.fr (C. Paillard).

Mouritsen et al., 2005; Soniat and Brody, 1988; Studer et al., 2013; White et al., 1988) and the results of these studies suggested that parasite prevalence and intensity reflected the combined effect of many biological and environmental controls.

In the 1990s, a host–parasite model for the eastern oyster (*Crassostrea virginica*) and the pathogen *Perkinsus marinus*, cause of Dermo disease, was developed (Hofmann et al., 1995; Powell et al., 1994, 1996). More recently, a second oyster parasite, *Haplosporidium nelsoni*, cause of MSX disease, was modeled (Ford et al., 1999; Paraso et al., 1999; Powell et al., 1999). Both *P. marinus* and *H. nelsoni* are water borne protozoans that infect and proliferate within the tissues of oysters, eventually reaching lethal proportions. Model-based investigations of these two systems focused on quantifying the relative contribution of specific environmental and biological factors in determining the outcome of the host–parasite interaction.

Other molluscan pathogens act in a different manner to disrupt life functions and eventually kill the host. One such pathogen is the bacterium, *Vibrio tapetis*, which causes Brown Ring Disease (BRD) in the Manila clam, *Venerupis* (= *Tapes*, = *Ruditapes*) *philippinarum* in western Europe (Borrego et al., 1996; Paillard, 2004b; Paillard et al., 1994). The bacterium producing BRD does not directly enter the clam tissues. Rather, it first adheres on the periostracal lamina, a sheet of organic material or conchiolin, which is composed mainly of complex proteins and polysaccharides. It is secreted by the mantle edge, which provides the substrate for mineralization (Paillard and Maes, 1995a). Colonization of the periostracal lamina by *V. tapetis* alters its structure, resulting in the deposition of a characteristic ring of conchiolin around the inner edge of the valves (Paillard et al., 1994).

The Manila clam is commercially harvested in Europe from the British Isles to the Mediterranean Sea (Goulletquer, 1997). The first outbreak of BRD was described in northern Brittany, France, in 1987 and it has since spread throughout the European growing regions where it has severely disrupted culture, and to a lesser extent wild harvests, of this species (Paillard, 2004b). The factors favoring BRD outbreaks in Manila clams are not well understood, but changes in environmental conditions such as temperature and food supply, and of biological factors including condition, hemocyte number and phagocytic capacity, and shell repair capability have been suggested as underlying causes (Allam et al., 2001; Paillard et al., 2004; Plana et al., 1996; Reid et al., 2003; Trinkler et al., 2010a). To evaluate the relative effects of these potential causes in the development of BRD in Manila clams, we developed a numerical model that simulates the host–parasite–environment relationship in this disease. The model also provides a framework for synthesizing and integrating the diverse data sets on Manila clam growth and physiology with equivalent data sets for *V. tapetis*.

The host portion of the model is based on one developed for the hard clam *Mercenaria mercenaria* (Hofmann et al., 2006a), modified and refined for *V. philippinarum* (Flye-Sainte-Marie et al., 2007a). Some of the basic concepts found in the oyster-pathogen models mentioned above were used in developing the clam-bacterium model, but the latter differs in significant ways. Rather than tracking a 'standard' host and then scaling results to clams of different sizes, the BRD model simulates host–parasite interactions for individual clams differing in phenotypes associated with the development of, and recovery from, BRD. In contrast to MSX and Dermo diseases, which involve the soft tissues of the oysters, host–pathogen interactions in BRD take place primarily in the extrapallial cavity, between the mantle and the inner shell, where the bacterium *V. tapetis* colonizes the conchiolin and disrupts the normal production of this layer. In addition, the intensity of BRD is scored using a symptom (the brown deposit intensity) (Paillard and Maes, 1994) and not by the density of pathogen. Finally, the BRD model differs from the oyster models in that the cellular defense system of the clam (hemocyte activity and shell recovery or nacrezation process) (Cheng, 1967), which is thought to play a prominent role in the disease outcome, is explicitly included as a model variable.

The objectives of this paper are then twofold. The first is to describe an individual-based BRD model that includes the capabilities of variable host phenotype and simulation of a disease caused by a pathogen that acts largely outside of the host's soft tissues and is defined by a symptom. The second is to use simulations to test hypotheses about the host–pathogen interactions thereby improving understanding of a disease process that is difficult to quantify in experimental and field settings. Consequently, the simulation results have direct implications for designing laboratory and field sampling programs that measure BRD in Manila clams and ultimately can be used to inform management practices for this commercial species. The framework and scaling conventions used in the BRD model are described in the following section. This is followed by descriptions of the model governing equations and parameterizations. Results from simulations are then described and the discussion section places the results in the context of what is known about diseases of marine bivalves in general and BRD in particular. The implications of differences between BRD and other marine bivalve diseases, and the accompanying assumptions, are evaluated through simulations with the host–pathogen model.

2. Background for model development

2.1. Overview of BDR and model conceptual basis

Although BRD in *V. philippinarum* is distributed along the Atlantic coast of Europe from Norway and England to Spain, it is most often found in northern countries and for this reason BRD is considered a cold-water disease (Paillard, 2004b; Paillard et al., 2008). Prevalences are typically higher in cultured clams (30 to 60%) than in wild stocks (10 to 30%) (Fig. 1). In both cultured and natural clam populations, BRD is more frequently observed in adult clams (25–50 mm) than in juveniles (10–25 mm) (Flye-Sainte-Marie et al., 2009b; Paillard, 1992). Seasonal prevalence patterns are clearly observed in cultured groups,
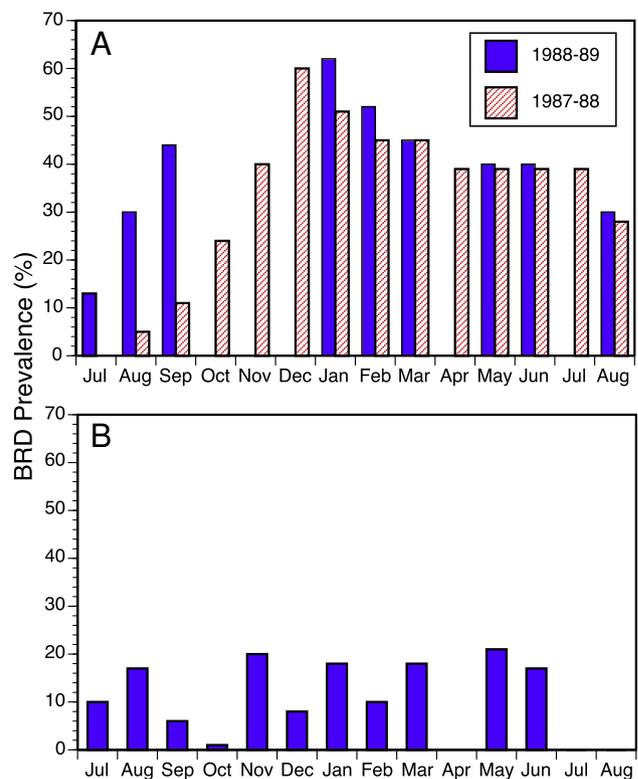

Fig. 1. Seasonal Brown Ring Disease prevalence patterns in (A) cultured and (B) wild Manila clams, *Venerupis philippinarum*. A. Data collected at a clam farm in Landeda, northern Brittany, France in 1987–88 and 1988–89. B. Average of data collected in the Gulf of Morbihan, Brittany, France in 1993, 94, 98, and 2000 to 2003.

with maxima most often in the winter and spring after settlement (Fig. 1). Seasonal cycles are more difficult to discern in natural populations and in some years no particular pattern has been measured (Flye-Sainte-Marie et al., 2009b).

The development of BRD in clams and *V. tapetis* infection strategies have been reviewed by Paillard (2004b) and Paillard and collaborators (1994). Here we consider only information pertinent to the model. Infections are initiated by the attachment of *V. tapetis* onto the periostracal lamina of the host clam (Paillard and Maes, 1995b) (Fig. 2). They can theoretically occur any time the clam is filtering, but environmental conditions at the time may modulate proliferation of the bacterium, as well as development of the symptom and its repair. The bacterium proliferates along the conchiolin and in the extrapallial fluid (Allam et al., 1996), severely disrupting the production of conchiolin and resulting in the anomalous deposit around the edge of the inner shell (Paillard and Maes, 1995a). As the disease progresses, the attachment of the mantle to the shell along the pallial muscle is severed, the bacteria enter the central extrapallial cavity, and the symptomatic conchiolin deposit becomes extended over most of the inner valves (Paillard and Maes, 1994). The presence of the brown ring itself is not considered to cause mortality unless it becomes very thick and extensive. Rather, most mortality is hypothesized to occur when the bacterium breaches the pallial muscle attachment, colonizes the central extrapallial fluid, penetrates lesions in the epithelium, and proliferates inside the tissues (Allam et al., 2002b; Paillard, 2004b).

Clams can recover from BRD through two hypothesized defense mechanisms. The first involves control of bacterial proliferation by hemocytes capable of phagocytosing the bacterium and anti-bacterial enzymes such as lysozyme, which are present in the extrapallial fluid, as well as in the hemolymph, of *V. philippinarum* (Allam and Auffret, 2000; Allam and Paillard, 1998). Enhanced phagocytic activity has been linked to resistance to experimental challenge (Allam et al., 2001). The second defense mechanism invokes shell repair through the deposition of calcium carbonate (CaCO$_3$) over the conchiolin, which sequesters bacteria under a layer of shell (Trinkler et al., 2010a, b, 2011a,b).

The BRD model developed in this study simulates the in vivo processes that occur during *V. tapetis* host colonization, multiplication and transmission to other clams. The model includes equations that describe the proliferation of the bacterium, the appearance and intensification of the conchiolin deposit, and the recovery of the clam by hemocyte
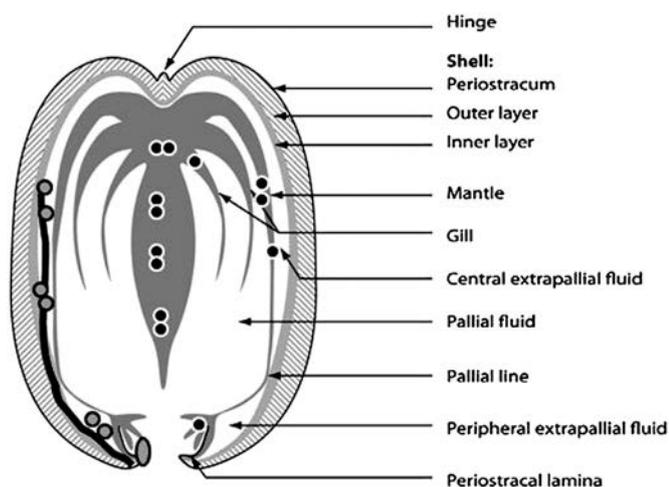
activity or CaCO$_3$ deposition over the deposit and attached bacteria, or the eventual death of clams if recovery mechanisms are ineffective (Fig. 3). Inclusion of phagocytosis and shell repair as recovery mechanisms allows the relative contribution of each to be evaluated.

The equations used to model the host and pathogen processes are derived from both field and laboratory studies. Most of the latter involved in vitro-cultured bacteria administered using known doses to clams held under controlled conditions. The BRD model relies on basic physiological processes of both host and parasite, as well as environmental factors (Fig. 4), to reproduce observed seasonal cycles of BRD prevalence and intensity, and of clam mortality, as has been done with other shellfish host–pathogen models (e.g. Powell et al., 1996). The BRD model, however, provides an advance in that it simulates the outcome of the host–parasite interaction for individuals of many different phenotypes. The latter allows inferences to be made about the effects of ranges of physiological conditions on susceptibility of individuals to infection and their ability to recover from infections.

The clam component of the BRD model includes parameterizations for filtration, respiration, the allocation of energy into reproductive and somatic tissues, and phagocytic rates (Allam et al., 2002a; Flye-Sainte-Marie et al., 2007a; Goulletquer, 1989; Soudant et al., 2004). These processes are modified by environmental temperature and food concentrations (Fig. 4). The food supply and filtration rate determine soft tissue condition index, which in turn determines clam growth and affects the abundance of hemocytes available for phagocytosis of bacteria (Soudant et al., 2004). The bacterial component of the BRD model includes parameterizations for the growth and death of the pathogen. These processes are modified by temperature and are indirectly affected by food supply via its effect on clam condition and the host defense system (Fig. 4). Transmission of *V. tapetis* between individuals is included and depends on the clam density, the severity of BRD and the concentration of *V. tapetis* in the population into which uninfected clams are introduced. Details of the equations used to simulate the host and pathogen processes are given in Section 3.

2.2. Model framework

The available information on BRD suggests that the host–pathogen response can be mediated by the physiological capability of the clam for assimilation, shell repair, and hemocyte response (Allam et al., 2001; Soudant et al., 2004; Trinkler et al., 2011a,b). Thus, the BRD model uses a three-dimensional framework that is developed around these three aspects of clam physiology. We do not know if these three parameters are genetically linked, but the simplest assumption for the purposes of the model is that they are not and that all may occur with some probability.

Fig. 2. Diagramatic representation of a cross-section of a Manila clam showing the infection process by *Vibrio tapetis*. Bacteria (gray spots) first adhere to the periostracal lamina, which causes that structure to rupture and the bacteria to enter and colonize the extrapallial fluid. The clam reacts by depositing brown conchiolin between the mantle and inner shell surface (dark line). If lesions are formed on the mantle or gill epithelium, bacteria can enter and multiply within the soft tissues (black spots). Adapted from Paillard (2004a,b)
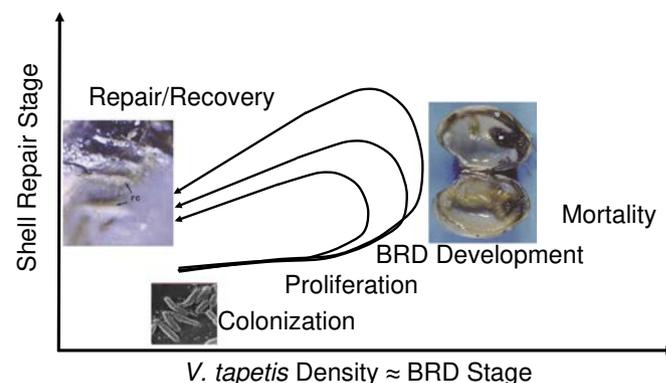

Fig. 3. Conceptual model of the Brown Ring Disease progression and repair process. Different line trajectories represent different possible outcomes depending on phenotypic ability to combat the disease agent, *Vibrio tapetis*, and to cover (repair) the conchiolin deposit characteristic of the disease.
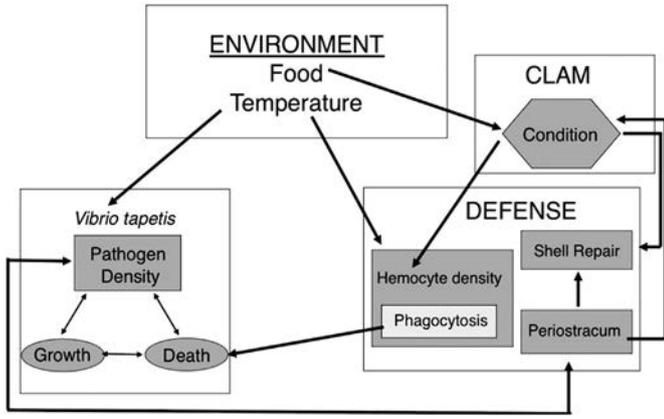
Fig. 4. Model linkages showing the major relationships among host, parasite, and environment in the Brown Ring Disease model.
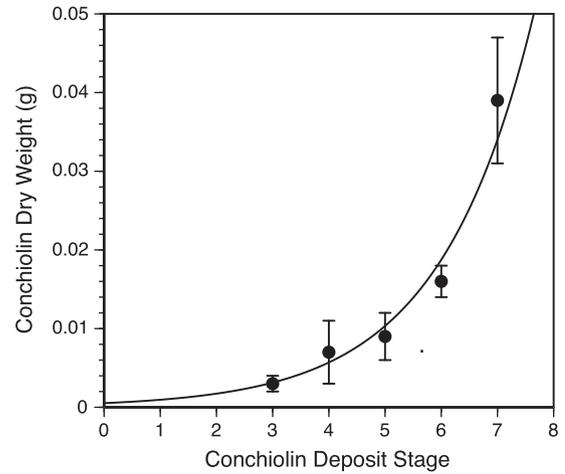

Fig. 5. Relationship between CDS (Conchiolin Deposit Stage) and the weight of conchiolin deposited on the inner shells of *Venerupis philippinarum* affected by Brown Ring Disease. The weight is for the deposit on both valves.

Assimilation is the incorporation of energy derived from food to produce tissue (= condition) and is dependent on food availability, filtration rate and assimilation efficiency (Flye-Sainte-Marie et al., 2007a). Shell repair is the amount of $CaCO_3$ laid down over the BRD deposit and depends on clam condition and the amount of conchiolin present. Hemocyte response is determined by the hemocyte density in the extrapallial fluid, the proportion of phagocytically active hemocytes, and the estimated number of bacteria per day that can be ingested by each hemocyte. This structure allows differentiation of the relative contribution of clam condition (via assimilation) and the two recovery processes on simulated disease prevalence and intensity, and ultimately on clam mortality. The approaches and conversions needed for development of this three-dimensional framework from laboratory and field observations are described in the following sections.

2.3. BRD classification scheme

The severity of BRD in clams is scored as the extent of the conchiolin deposit and whether there is evidence of recovery in the form of $CaCO_3$ layered over the deposit (Paillard and Maes, 1994). The Conchiolin Deposit Stage (CDS) is scored from 0 to 7 with 7 having the most extensive deposit. The Shell Repair Stage (SRS) is scored from 0 to 3, with 3 being a shell with brown deposit completely covered by shell layers. The relationships described below allow the model results to be expressed in terms of CDS and SRS so that comparisons between simulated BRD stages and those observed in field and laboratory studies can be made.

The staging system for the BRD symptom is based on the area coverage and the relative thickness of the conchiolin deposit (Paillard and Maes, 1994). To use this staging system for evaluation of model results, quantitative data relating the BRD stage with the amount of conchiolin present were obtained using archived clam valves (mean length 33.2 mm ± SE, 0.74). Valves that represented CDS 3–7 were selected, and the conchiolin was scraped off and weighed (stages less than 3 had too little conchiolin to scrape off and weigh) to provide an estimate of the amount of conchiolin for each stage. The CDS-conchiolin weight data were then used to develop an empirical relationship (Fig. 5) that converts conchiolin weight, the value obtained from the model, to CDS as

$$CDS(\hat{P}) = CDS_0 + CDS_1\hat{P} + CDS_1\hat{P} + CDS_2\hat{P}^2 + CDS_3\hat{P}^3 + CDS_4\hat{P}^4 \quad (1)$$

where $\hat{P}$ is conchiolin weight (P) scaled to the shell area of 33-mm clam (ShA_{33}) as

$$\hat{P} = \left(\frac{ShA33}{ShA}\right)P. \quad (2)$$

ShA is described in Section 2.5. Throughout the model development a 33-mm clam is used as a reference point because this is the mean shell length of clams used to obtain the relationship of conchiolin deposit weight to CDS. It represents an adult clam and is close to market size (35 mm) in France. The shell area covered by conchiolin changes over time and the determination of this area is described in Section 3.5. Equation coefficient values are given in Table 1

The quantity of $CaCO_3$ layered over the conchiolin deposit for the 5 shell repair stages (SRS) (Paillard, 2004b) was estimated to provide a relationship to convert model output to SRS. Valves of known size were weighed to obtain a relationship between weight and a surface area. From the density of $CaCO_3$ in seawater (2.93 g cm^{-3}) and the approximate surface area of a valve, the weight of $CaCO_3$ per mm^2 of shell surface was computed. The thickness of the $CaCO_3$ layer over the conchiolin deposits was estimated from photomicrographs as being between 60 and 100 μm thick (Paillard, 1992). For a 100 μm-thick layer, the weight of $CaCO_3$ for each mm^2 of coverage is then 293 μg. This $CaCO_3$ weight and the estimated percent coverage for each SRS category (Fig. 6) provided the relationship between grams of $CaCO_3$ covering the organic deposit and SRS.

Using this empirical relationship, SRS was defined in terms of the weight of $CaCO_3$ (Ca) deposited, also scaled to the shell area of a 33-mm clam as

$$\hat{Ca} = \left(\frac{ShA_{33}}{ShA}\right)Ca \quad (3)$$

and SRS is defined by

$$SRS(\hat{Ca}) = SRS_0 + SRS_1\hat{Ca} + SRS_2\hat{Ca}^2 \quad (4)$$

where SRS is between 0 and 3. Coefficient values are given in Table 1.

2.4. Disease stage conversion to bacterial density

The BRD model operates on the basis of the pathogen concentration in the extrapallial fluid. Therefore, a relationship was developed to relate the density of *V. tapetis* in the extrapallial cavity to disease stage so that simulation results could be compared to observations. Extrapallial fluid was collected from a set of experimentally challenged clams that exhibited different CDS and SRS after a 60-day exposure (Ford and Paillard, 2007). Bacterial concentrations were estimated using a monoclonal antibody (Nöel et al., 1996) and grouped into 6 classes (Table 2), which were then plotted against CDS and SRS (Figs. 7 and 8). The

Table 1
Units, definitions and values of parameters and coefficients used in the equations that provide the conversion of model results to CDS (Conchiolin Deposit Stage) and SRS (Shell Repair Stage) and those that are used to obtain clam dry flesh weight from shell length. See Eqs. (1)-(8) in the text.

Parameter or coefficient	Units	Definition	Value
CDS_0	No units	Conchiolin weight-CDS stage conversion equation coefficient	3.920×10^{-3}
CDS_1	g^{-1}	Conchiolin weight-CDS stage conversion equation coefficient	1.001×10^3
CDS_2	g^{-2}	Conchiolin weight-CDS stage conversion equation coefficient	-6.458×10^3
CDS_3	g^{-3}	Conchiolin weight-CDS stage conversion equation coefficient	1.946×10^6
CDS_4	g^{-4}	Conchiolin weight-CDS stage conversion equation coefficient	-2.132×10^7
ShA_{33}	mm^2	Shell area (both valves) of 33-mm shell length clam	1.566×10^3
SRS_0	No units	CaCO3 weight deposition-SRS stage conversion equation coefficient	-1.473×10^{-2}
SRS_1	g^{-1}	CaCO3 weight deposition-SRS stage conversion equation coefficient	10.295
SRS_2	g^{-2}	CaCO3 weight deposition-SRS stage conversion equation coefficient	-8.186
a_o	g	Coefficient of allometric equation relating clam dry flesh weight to shell length	8.518×10^{-11}
bo	No units	Coefficient of allometric equation relating clam dry flesh weight to shell length	3.728
a_m	g	Coefficient of allometric equation relating maximum clam dry flesh weight to shell length	1.703×10^{-12}
bm	No units	Coefficient of allometric equation relating maximum clam dry flesh weight to shell length	3.728
W_o	g	Mean dry flesh weight for a given clam length	Calculated
W_{max}	g	Maximum dry flesh weight for a given clam length	Calculated
h_o	mm	Clam shell length to height equation coefficient	4.524
h_1	mm	Clam shell length to height equation coefficient	0.582

threshold for clam mortality is about CDS 4 (Paillard and Ford, unpublished). At this stage, the conchiolin deposit covers most of the edge of the inner valve and is beginning to extend to the valve surface underlying the siphons and the central extrapallial compartment (Paillard and Maes, 1994). If a clam can control bacterial proliferation and begin to cover the conchiolin deposit before CDS exceeds 4, it can usually recover. If not, bacteria continue to multiply, the organic deposit becomes more pronounced, the condition index decreases, bacteria have a greater chance of penetrating the soft tissues, and the clam is much more likely to die (Allam et al., 2002b; Flye-Sainte-Marie et al., 2007b; Paillard, 1992).

2.5. Clam weight and condition

All morphometric values used to evaluate clam condition were obtained from a dataset collected during an earlier study (N = 921, $r^2 = 0.904$; Paillard, 1992). Mean dry flesh weight (W_o) was obtained from length (L — maximum anterior–posterior dimension)

$$W_o(L) = a_o L^{bo} \tag{5}$$

where a_0 and bo are constant parameters (Table 1). Similarly, maximum weight (W_{max}) was obtained from length as

$$W_{max}(L) = a_m L^{bm} \tag{6}$$

where a_m and bm are constant parameters (Table 1).
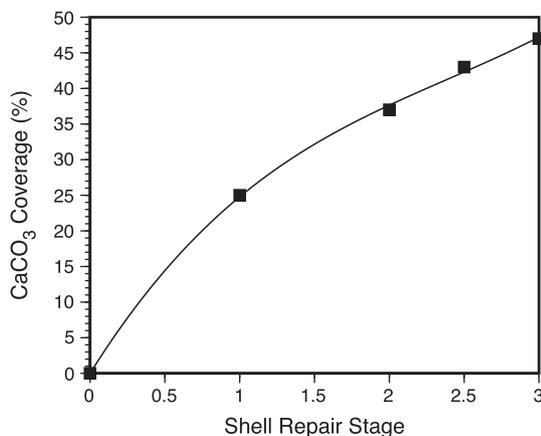

Fig. 6. Estimated relationship between percent CaCO3 coverage and SRS (Shell Repair Stage) in *Venerupis philippinarum* affected by Brown Ring Disease.

In the model, clam condition (C) is a relative term and is defined as a function of the current weight (W) of each individual clam compared to the mean and maximum weights for that clam's current length (Table 1)

$$C(W, L) = \frac{W - W_o(L)}{W_{max}(L) - W_o(L)}. \tag{7}$$

A clam with the mean weight for its length has a condition of zero and a clam at maximum weight for its length has a condition of 1. A clam below the mean weight has a negative condition and no lower bound is set for poor condition.

Clam height (H — umbo to ventral margin) was estimated from length as

$$H = h_o + h_1 L \tag{8}$$

where h_0 and h_1 are constant parameters (Table 1). Clam height and length were used to define shell area (ShA) of both valves as $2HL$.

3. Model processes and relationships

3.1. Governing equations

The BRD model consists of coupled equations (parameters, units, values and coefficients are given in Tables 1, 3 and 4) that describe changes in clam weight (W, gm), clam length (L, mm), clam condition (C, no units), *V. tapetis* concentration (V, cells mL^{-1}), conchiolin weight (P, gm), and CaCO3 (Ca, gm) deposition as a function of time (t) as

$$\frac{d}{dt}[W, L, C, V, P, Ca] = [R_W, R_L, R_C, R_V, R_P, R_{Ca}] \tag{9}$$

Table 2
Allocation of *Vibrio tapetis* densities in *Ruditapes philippinarum* extra-pallial fluid into classes as determined by ELISA.

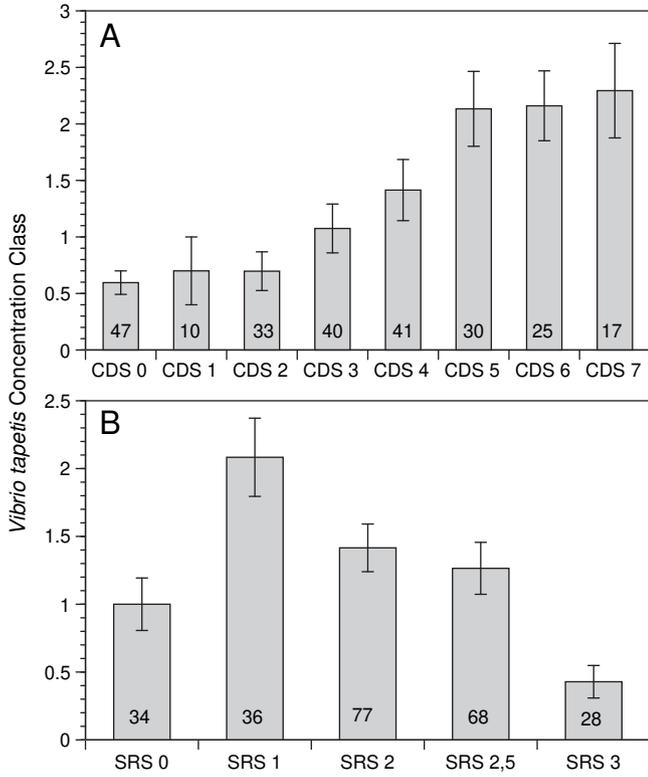| ELISA class	*V. tapetis* concentration (cells mL^{-1})
0	$\leq 5 \times 10^4$
1	$5 \times 10^4 - 1 \times 10^5$
2	$1 \times 10^5 - 2.5 \times 10^5$
3	$2.5 \times 10^5 - 5 \times 10^5$
4	$5 \times 10^5 - 7.5 \times 10^5$
5	$7.5 \times 10^5 - 1 \times 10^6$
6	$\geq 1 \times 10^6$

Fig. 7. Relationship between *Vibrio tapetis* concentration classes and two measures of Brown Ring Disease in *Venerupis philippinarum*: A. CDS (Conchiolin Deposit Stage) and B. SRS (Shell Repair Stage). See Table 2 for description of *V. tapetis* concentration classes, which were estimated using a monoclonal antibody assay (ELISA).

where R_w, R_L, R_C, R_V, R_P and R_{Ca} represent the processes that provide gains and losses for each model variable. Details of the simulation of changes in clam weight, length and condition are given in Flye-Sainte-Marie et al. (2007a). Only those used in the BRD model are described here. These include details of the simulated changes in *V. tapetis* concentration, conchiolin weight, and CaCO$_3$ deposition.

3.2. V. tapetis concentration change

The change in *V. tapetis* concentration was assumed to be controlled by bacterial growth (V*grow*) and death (V*death*) resulting from hemocyte activity and temperature (VHD) as:

$$R_V(R, V, C, t) = Vgrow(T, V)V - Vdeath(T, V, C, t) - VHD(T)V \qquad (10)$$

where growth rate is controlled by temperature (T) and *V. tapetis* cell concentration (V), and mortality has an additional dependence on clam condition (C), which affects hemocyte concentration (Fig. 4).

3.2.1. V. tapetis growth

In vitro, *V. tapetis* proliferation rates are dependent on temperature (Paillard, 2004a) and bacterial density. Therefore, in the simulated growth of *V. tapetis*, the base growth rate (V*g*) is modified by temperature (VgT) and bacterial density (V):

$$Vgrow(T, V) = Vg VgT(T) \frac{1}{(V \times 10^{-6})^{3/2}}. \qquad (11)$$

This "crowding effect" occurs in vitro when cultures reach the stationary phase and is presumed to occur in vivo (Paillard, unpublished). The upper range of measured *V. tapetis* densities, determined by an ELISA test, in the extrapallial fluid is $\geq 10^6$ cells mL^{-1} after experimental challenge (Allam et al., 2002b) (Table 2). Therefore, 10^6 cells mL^{-1} was assumed to represent the concentration at which *V. tapetis* proliferation becomes affected by crowding and the simulated bacterial growth rates were decreased above this value, assuming a $-3/2$ volume-to-surface law dependence.

The optimum temperature for growth of isolates from several sites in France is 21 ± 2 °C, with growth decreasing to zero at 1 and 27–30 °C (Paillard, 2004a; Paillard et al., 1997). These observations were used to describe the temperature dependence of *V. tapetis* growth (VgT) as

$$VgT(T) = \frac{2(1 + VgT_o) * TF(T)}{TF(T)^2 + 2VgT_o TF(T) + 1} \qquad (12)$$
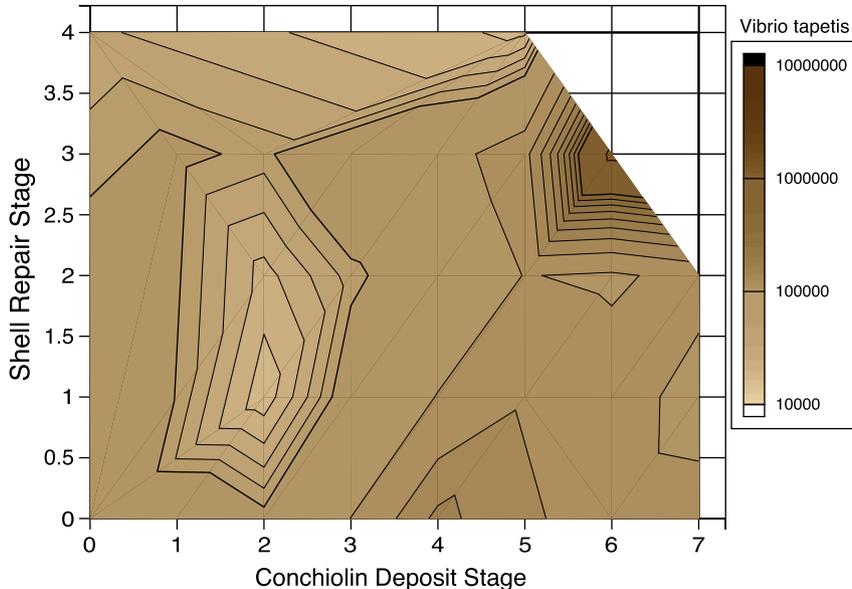

Fig. 8. Observed relationship of CDS (Conchiolin Deposit Stage), SRS (Shell Repair Stage) and *Vibrio tapetis* density in *Venerupis philippinarum* showing the variation in bacterial density for each CDS and SRS stage.

6

Table 3
Units, definitions and values of parameters and coefficients used in the equations that describe *Vibrio tapetis* growth, mortality and virulence. See Eqs. (10)–(21) in the text.

Parameter or coefficient	Units	Definition	Value
V_g	d^{-1}	Maximum daily *V. tapetis* growth rate	0.6
VgT_o	No units	Baseline *V. tapetis* growth rate	-0.6
TF_1	°C	Maximum temperature for *V. tapetis* growth	30
T_{opt}	°C	Optimum temperature for *V. tapetis* growth	21
TF_o	°C	Minimum temperature for *V. tapetis* growth	1
H_{ing}	Cells d^{-1}	Daily ingestion rate of *V. tapetis* per hemocyte	1
K_H	Cells mL^{-1}	Half saturation coefficient for hemocytes in extrapallial fluid	9×10^5
c_o	mL $cell^{-1}$	Coefficient in equation relating hemocytes concentration to clam condition	0.5928
H_o	Cells mL^{-1}	Mean hemocyte concentration in extrapallial fluid	2.6×10^6
H_m	Cells mL^{-1}	Maximum hemocyte concentration in extrapallial fluid	4.8×10^6
H_r	mL $cell^{-1}$	Coefficient that increases the hemocyte concentration due to *V. tapetis* density	10^{-5}
Td	°C	Temperature at which hemocyte activity ceases	43
To	°C	Optimum temperature for ingestion of *V. tapetis* by clam hemocytes	17
m	No units	Exponent in relationship of temperature to ingestion rate of *V. tapetis* by hemocytes	1.529
n	No units	Exponent in relationship of temperature to ingestion rate of *V. tapetis* by hemocytes	2.3
HAmax	No units	Maximum proportion of phagocytically active hemocytes	0.75
HAmin	No units	Minimum proportion of phagocytically active hemocytes	0.001
HAvmin	Cells mL^{-1}	Threshold *V. tapetis* concentration that drives phagocyte activity up or down	5.0×10^4
HAg	d^{-1}	Constant in equation that determines how rapidly phagocyte activity increases with increased exposure to *V. tapetis*	0.2
HAvscale	Cells mL^{-1}	Concentration of *V. tapetis* needed to activate hemocytes	2.5×10^6
VV_o	No units	Coefficient of *V. tapetis* virulence	-0.1487
VV_1	No units	Coefficient of *V. tapetis* virulence	-0.0594
VV_2	No units	Coefficient of *V. tapetis* virulence	0.0013
VV_3	No units	Coefficient of *V. tapetis* virulence	-9.61×10^{-6}
T_m	°C	Temperature above which the probability of *V. tapetis* death is 0.5	27

where the temperature factor (TF) varies above and below the optimum temperature (T_{opt}, Table 3) as

$$TF(T) = \begin{cases} \dfrac{T - TF_1}{T_{opt} - TF_1} & \text{for } T \geq T_{opt} \\ \dfrac{T - TF_o}{T_{opt} - TF_o} & \text{for } T < T_{opt} \end{cases}. \tag{13}$$

The relationship given by Eq. (12) (Fig. 9A) scales the temperature dependence of growth so that the simulated growth rates match the patterns of observed rates.

3.2.2. V. tapetis death

The removal rate of *V. tapetis* by hemocytes is assumed to be governed by the equation

$$\begin{aligned} &Vdeath(T, V, C, t) \\ &= HC(V, C) H_{ing} \frac{HIT(T)}{HIT(15)} \left(\frac{V}{K_H + V} \right) HA(t, V) VV(V, C) \end{aligned} \tag{14}$$

where the terms on the right side of Eq. (14) represent the hemocyte concentration (HC) in the extrapallial fluid, the rate of elimination of *V. tapetis* by hemocytes (H_{ing}), modification of hemocyte activity based on temperature (HIT), *V. tapetis* virulence (VV), clam hemocyte activity (HA) and *V. tapetis* virulence (VV), respectively. Details of the data and parameterizations used to develop these relationships are as follows.

3.2.2.1. Hemocyte concentration. The density of hemocytes in the extrapallial fluid of *V. philippinarum* (Allam and Paillard, 1998) increases in direct relationship with the severity of BRD (Allam et al., 2000; Oubella et al., 1993). Clams with higher condition index also have higher densities of hemocytes in the hemolymph (Soudant et al., 2004) and this relationship was assumed to be true for extrapallial fluid hemocytes. Given these observations, the parameterization for hemocyte concentration (HC) was assumed to be dependent on clam condition index (C) and *V. tapetis* concentration, such that it increased with increasing condition, and increased bacteria concentration

$$HC(V, C) = 10^{(coCHC_o(V))} \tag{15}$$

where $HC_o(V)$ is

$$HC_o(V) = H_o + (H_m - H_o)\left(1 - e^{-HrV}\right) \tag{16}$$

and the coefficient values are given in Table 3.

3.2.2.2. Hemocyte activity. Extrapallial fluid hemocytes can readily phagocytose *V. tapetis* (Allam et al., 2001, 2002b). The proportion of hemocytes found to have phagocytosed *V. tapetis* in vivo and in vitro ranged between 10 and 40% (Allam and Ford, 2006; Allam et al., 2001, 2002b). But, measurements of the elimination rate of injected *V. tapetis* (virulent strain, isolate P16) from the hemolymph of *V. philippinarum* suggest that a removal rate of one bacterium per

Table 4
Units, definitions and values of parameters and coefficients used in the equations that describe shell repair. See Eqs. (22)–(28) in the text.

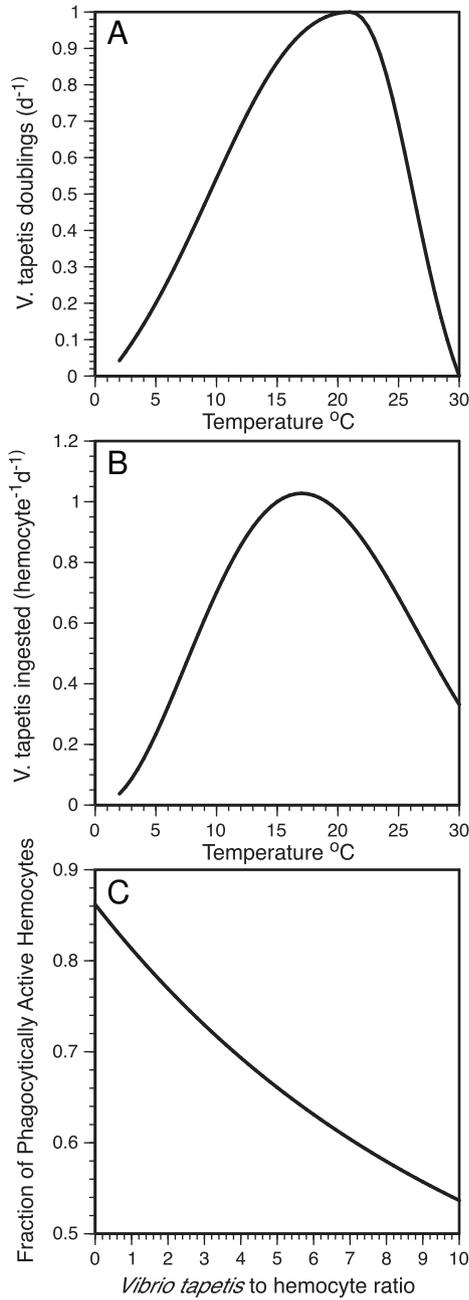| Coefficient or Parameter	Units	Definition	Value
P_g	d^{-1}	Maximum conchiolin deposition rate	6.0×10^{-5}
K_p	Cells mL^{-1}	*V. tapetis* concentration at which the rate of conchiolin deposition is one-half the maximal rate, P_g	5.0×10^4
W_r	g	Dry flesh weight of reproductive tissue	Calculated
W_{33}	g	Dry flesh weight of 33-mm shell length clam	0.5
Cb	No units	Clam weight dependency on conchiolin and $CaCO_3$ deposition rates	0.4766
C_g	d^{-1}	Maximum $CaCO_3$ deposition rate	4.9×10^{-3}
K_c	g	Conchiolin concentration at which the rate of $CaCO_3$ deposition is one-half the maximal rate, C_g	0.01
PSD	g mm^{-2}	Weight per area of conchiolin	2.554×10^{-5}
CSD	g mm^{-2}	Weight per area of $CaCO_3$	2.93×10^{-4}

Fig. 9. Simulated relationships of factors affecting the interaction between *Vibrio tapetis* and Manila clams: A. temperature effects on *V. tapetis* proliferation rate; B. temperature effect on ingestion rate of *V. tapetis* by clam hemocytes; and C. virulence of *V. tapetis* as a function of hemocyte to bacterial ratio.

bacteria were immediately ingested. Thus, an activity factor (HA), which defines the proportion of hemocytes that are phagocytically active at any time, was included to delay initiation of bacterial ingestion by hemocytes as

$$\frac{d}{dt}\mathrm{HA}(t,V) = \begin{cases} \mathrm{HA}_r(V)(\mathrm{HA}max - \mathrm{HA}) & \text{for } V > \mathrm{HA}vmin \\ 10\mathrm{HA}_r(V)(\mathrm{HA} - \mathrm{HA}min) & \text{for } V < \mathrm{HA}vmin \end{cases} \tag{18}$$

where HAmin and HAmax determine the upper and lower bounds of the proportion of phagocytically active hemocytes (Table 3). This relationship increases or decreases phagocyte activity in response to the current *V. tapetis* concentration where the activity change rate (HA$_r$) is

$$\mathrm{HA}_r(V) = \mathrm{HA}_g \frac{V - \mathrm{HA}min}{\mathrm{HA}vscale}. \tag{19}$$

HAmin sets the minimum *V. tapetis* concentration (Table 3) at which hemocyte activity will start to increase and HAvscale (Table 3) controls how rapidly it will increase. The proportion of phagocytically active hemocytes is low during early stage infections, when bacterial concentrations are low, and increases as concentrations increase.

3.2.2.3. V. tapetis virulence. A "virulence" factor was included to decrease the proportion of phagocytically active hemocytes as the density of bacteria increases. *Vibrio* virulence (VV) is estimated from experimental evidence showing a cytotoxic effect of *V. tapetis* on hemocytes of *V. philippinarum*, which is positively related to the ratio of bacteria to hemocytes (Choquet et al., 2003). The virulence effect was included by decreasing the proportion of phagocytically active hemocytes with increasing bacteria density as

$$\mathrm{VV}(V,C) = e^{\left(\mathrm{VV}_o + \mathrm{VV}_1 \cdot \mathrm{VHR} + \mathrm{VV}_2 \cdot \mathrm{VHR}^2 + \mathrm{VV}_3 \cdot \mathrm{VHR}^3\right)} \tag{20}$$

where VHR is the ratio of *V. tapetis* to hemocytes and is calculated at each model time step (Fig. 9C). The value of the virulence factor is taken as the larger of 0.32 or the value obtained from Eq. (20). This ensures that the virulence has a minimum value, which allows *V. tapetis* to always have an effect on the clams. The coefficient values for Eq. (20) (Table 3) and the virulence minimum were set based on observations (Choquet et al., 2003).

3.2.2.4. Temperature. Most *V. tapetis* strains die as temperature increases in vitro. The bacterium ceases to grow and survive at temperatures ≥27 °C and it is rapidly killed at 30 °C (Maes, 1992; Paillard et al., 1997). This temperature-dependent mortality (VHD) was imposed as

$$\mathrm{VHD}(T) = 0.5(1 + tanh(T - Tm)) \tag{21}$$

which provides increasing mortality with increasing temperature and total mortality above 27 °C (Fig. 9A).

3.3. Conchiolin deposition

Observations show a hyperbolic relationship between CDS and *V. tapetis* concentration in the extrapallial fluid of the clam (Fig. 7). These experimental data were used to develop a relationship that describes conchiolin deposition (R_p) as a function of the density of *V. tapetis* and the dry flesh weight (W) of the clam (scaled to a 33-mm clam, W_{33}) as

$$R_P(V,W) = P_g \left(\frac{V}{Kp + V}\right)\left(\frac{W - W_r}{W_{33}}\right)^{Cb} \tag{22}$$

where coefficient values are given in Table 4. The weight of reproductive tissue (W_r) is removed from the total dry flesh weight so that conchiolin deposition is dependent on somatic tissue normalized by the somatic

hemocyte per day is a reasonable base level (Allam et al., 2002b), and this rate was used as the base hemocyte ingestion rate.

Hemocyte density and phagocytic rates increase with increasing temperature (Allam et al., 2002a; Paillard, 2004b), therefore, base hemocyte ingestion rate was then modified by temperature (Fig. 9B) as

$$\mathrm{HIT}(T) = \left[\left(\frac{T_d - T}{T_d - T_o}\right)^m \left(\frac{T}{T_o}\right)\right]^n \tag{17}$$

where the coefficients are given in Table 3.

Preliminary simulations initiated with a single bacterium entering the extrapallial cavity produced no lasting infections because the

tissue of a 33-mm clam. This dependence on weight allows larger clams to have the capacity to cover their larger shell area.

3.4. Calcium carbonate deposition

The rate at which $CaCO_3$ deposition (R_{Ca}) occurs was assumed to be controlled by the amount of existing conchiolin and the available shell area scaled to a 33-mm shell as

$$R_{Ca}(W, P, H, L, C) = \frac{C_g PCaF(W)}{K_c CaF(W) + P} min\left[1, 0.007\left(\frac{ShA}{ShA_{33}}\right)P^{-5}\right] \times \left(1 + 2\hat{C}\right)$$

(23)

where the minimum function constrains the deposition rate as the available shell area becomes large relative to that of 33-mm clam. The coefficient values are given in Table 4. Available shell area (ShA) is calculated as described in Section 3.5 and is scaled relative to the shell area of a 33-mm clam (ShA_{33}). The deposition is scaled relative to clam condition ($\hat{C}$). For positive condition, $\hat{C} = 0.5C$; for negative condition $\hat{C} = C$.

The dependence of $CaCO_3$ deposition on clam weight is given as

$$CaF(W) = \left(\frac{W - W_r}{W_{33}}\right)^{Cb}.$$

(24)

As in Eq. (23), the weight of reproductive tissue (W_r) is removed from the total dry flesh weight to calculate the weight dependency on $CaCO_3$ deposition. Once deposited, neither conchiolin nor $CaCO_3$ diminishes, except when SRS = 3 (repair complete) occurs. At this time, the model resets the disease stage and the clams revert to SRS 0.

3.5. Adjustments for changes in shell area

As the clam grows, shell area increases, which requires increased production of conchiolin and $CaCO_3$ to cover the larger surface. The increased production is converted to shell area covered by a factor that converts conchiolin (P) and $CaCO_3$ (Ca) weights to an equivalent area covered as, $PA = P$ / PSD and $CA = Ca$ / CSD, respectively. The PSD and CSD factors are weight per area of conchiolin and $CaCO_3$, respectively (Table 4). These conversion factors represent a fixed thickness of the conchiolin and carbonate material and are based on measurements made from thin sections of affected shells (Paillard and Maes, 1995b). The new surface area covered by conchiolin (dPA) or $CaCO_3$ (dCA) is calculated by difference in PA and CA over a specified time. The uncovered part of the shell (RA) that is available for coverage is calculated from the total shell area (ShA) minus the area already covered by PA and CA as, RA = ShA − PA − CA.

New conchiolin can be deposited on top of existing conchiolin (RA) or repaired shell (CA) (Trinkler et al., 2010a). The area covered by $CaCO_3$ at the end of specified time interval is calculated by adding the new production (dCA) to the existing covered area (CA) and removing the area covered by the new conchiolin, which covers new shell or repaired shell as

$$CA = CA + dCA - dPA\frac{CA}{CA + RA}.$$

(25)

Similarly, the new area covered by conchiolin is

$$PA = PA + dPA - dCA\frac{PA}{PA + RA}.$$

(26)

Shell repair is considered to be complete when the conchiolin deposit covers less than 1% of the shell area. The $CaCO_3$ weight is then set to zero.

The total weight of the conchiolin deposited in a specified time interval was limited by observations that indicated that a 33-mm clam can have a deposit of at most 0.04 g as

$$P = min\left[PA \ PSD, 0.04\left(\frac{ShA}{ShA_{33}}\right)\right]$$

(27)

where the total mass of conchiolin to be deposited is calculated from the area covered (PA) and the surface density of conchiolin (PSD). The maximum allowed mass of conchiolin is calculated relative to the shell area scaled to shell area of a 33-mm clam. The deposited conchiolin mass has to be less than or equal to this maximum. Similarly, the mass of $CaCO_3$ to be used for shell repair was limited to the maximum allowed mass, which was scaled relative to 0.4588 g for a 33-mm clam

$$Ca = min\left[CaCSD, 0.4588\left(\frac{ShA}{ShA_{33}}\right)\right].$$

(28)

Coefficient values are given in Table 4.

4. Modification of clam filtration rate by BRD

The digestive gland architecture and tissue biochemical composition are altered in clams affected by BRD (Plana and Le Pennec, 1991; Plana et al., 1996). The increasing thickness of the conchiolin deposited around the shell edge as the severity of BRD increases interferes with filtration (Flye-Sainte-Marie et al., 2007b) and may be responsible for at least part of these alterations. This impairment to filtration rate was incorporated into the clam growth model once CDS scores exceeded 2.5, and the effect becomes increasingly severe at CDS scores of 5–7 (Flye-Sainte-Marie et al., 2007b).

The effect of the BRD deposit on clam filtration (FPC) depends on the amount of conchiolin present scaled by the clam weight obtained from

$$FPC(P) - P\left(\frac{W_{33}}{W - W_r}\right)^{Cb}.$$

(29)

The reduction in filtration rate (FPF(P)) by the conchiolin is given by

$$FPF(P) = 1 - 12.5(FPC(P) - 0.003)$$

(30)

and is constrained to be between 0.5 and 1.

5. Cohort and population processes

The individual-based model provides simulations for ranges of parameter values that represent different phenotypes, as described in the next section. These individual-based model results were combined, based on the fraction of the population represented by a particular phenotype, to develop cohorts, which are equivalent to a year class. A Gaussian distribution was used to represent the contribution of the different phenotypes to the cohort; individuals with average characteristics are more common in the cohort than those at the extremes. This simulated cohort was used to determine the time change in presumed genetic composition due to differential mortality.

A representation of the population was obtained by combining individual cohorts produced by reproductive events that are dependent on the total population number. The disease characteristics of the individuals introduced into the population by a new cohort are determined by the population density and BRD infection intensity (see Section 6.3).

5.1. Phenotypic variation

The individual-based model was run for different values of three physiological parameters that affect clam health (assimilation), shell repair ($CaCO_3$ deposition), and hemocyte response (determined by hemocyte density, fraction of phagocytically active cells and daily

ingestion rate of bacteria). The mean values for assimilation efficiency and CaCO$_3$ deposition used to establish the reference simulation were 40% and 4.9×10^{-3} g clam^{-1} day^{-1}, respectively, for a 33-mm clam. The primary control is from the hemocyte ingestion rate, which for the base case simulation is 1 *V. tapetis* hemocyte^{-1} day^{-1}. These values were modified by a factor that ranged from 0.2 to 1.8. Similarly, the hemocyte response is the product of several processes and these are varied by multiplying the overall response by a factor that ranges between 0.2 and 1.8 (Fig. 10). The range was chosen to encompass all possible phenotypic values, and assumes a variance of ± 2 standard deviations (Hofmann et al., 2006b) from the mean, although very few individuals are found at either extreme. Simulations were done for individuals with every possible combination of these physiological values (9^3 simulations). These results provide the information that is used for analysis.

Cohorts were produced by combining and averaging the individual simulations. The physiological variations are not equally likely, so each simulation is weighted by the likelihood of being represented in the population because the number of individuals having each physiological type was assumed to follow a Gaussian distribution (Fig. 10). The properties derived from the simulations that relate to BRD, such as CDS and SRS, were calculated from the individual simulations using the Gaussian weighting.

The results of the individual simulations were combined into three subgroups representing high, intermediate and low performing phenotypes to investigate how phenotype variation affected the simulation results. The three categories were based on a percentage of the mean values as follows: low (L < 70%), intermediate (70% ≤ I ≤ 130%), and high (H > 130%). Thus an individual clam may fall into one of 27 subgroups in which assimilation, shell repair, and hemocyte response could range from high in all three categories to low in all three, with all possible combinations between (i.e., HHH, HHI, HIH ...... ILL, LIL, LLL).

5.2. Infection timing

For the cohort calculations, infections occurred in the middle of each month in the first two years of the clam life. As a control, one simulation was done in which no infection events occurred at all. The infection simulations were done for each combination of physiological parameter and phenotype class (25×9^3 simulations). The cohorts then combine
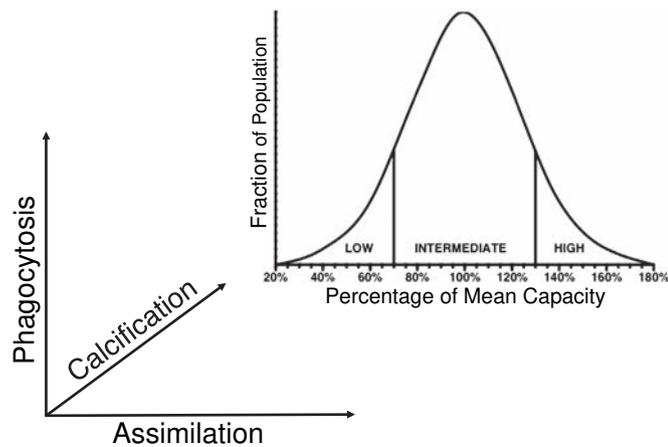

Fig. 10. Gaussian (normal) distribution showing the partitioning of high, intermediate and low performing phenotypes for the three physiological parameters used to vary model simulations: assimilation, CaCO$_3$ deposition and hemocyte activity in an unaffected clam. The mean is set at 100%. Each of the three axes contains the same distribution, so that each individual is placed in a 3-dimensional space. Mean values for the parameters are assimilation: 40% efficiency for a clam of 33 mm shell length; CaCO3 deposition: 4.9×10^{-3} g clam^{-1} day^{-1}; and hemocyte response is determined by hemocyte density, the fraction of phagocytically active cells and the daily ingestion rate of bacteria. The primary control on hemocyte response is hemocyte ingestion rate, which is estimated at 1 *V. tapetis* hemocyte^{-1} day^{-1}.

equal numbers of animals from each of the 25 infection classes using a Gaussian-weighted dependence that represent the number of individuals in each simulation. As a result, the cohorts include animals that are infected in every month of the year and equal representation of all possible infection times is assured.

5.3. Clam mortality

The severity of the conchiolin deposit is correlated with death. The ratio of dead to live clams rises above 1:1 when CDS ≥ 4 and is nearly 6:1 at CDS 6 (Paillard and Ford, unpublished). Heavy conchiolin deposits may interfere with filtration, which reduces condition and leads to mortality (Flye-Sainte-Marie et al., 2007b). The deposits may also irritate the mantle epithelium, allowing *V. tapetis* to penetrate into the tissue, where it causes death (Allam et al., 2002b). Also, the ability of hemocytes in the extrapallial fluid may be compromised at high *V. tapetis* densities, resulting in penetration into the soft tissues, even in some individuals without BRD signs (Paillard, 2004b). Low condition not caused by BRD (Paillard, 1992) and other, nonspecific, causes are also factors in mortality. From these observations, clam mortality was formulated as the sum of mortality resulting from *V. tapetis* density, CDS, condition index and nonspecific background mortality. The fraction of the clam population that dies each day from each source of mortality was calculated for each phenotype (see Section 6), summed, and removed from the population.

The clam mortality caused by exposure to *V. tapetis* (MV) is assumed to follow a relationship given by

$$MV(t, V) = \frac{MV_o}{2}\left[1 + tanh\left(\frac{MEV(V, t) - MEV_o}{MEV_1}\right)\right] \quad (31)$$

where the base mortality rate, MV_o, is set such that *V. tapetis* will reduce the clam population by 50% in 60 days (Table 5). This base rate is modified by a cumulative exposure to *V. tapetis* ($MEV(V,t)$) that is determined from the bacterial concentration. This response becomes active at a threshold (MEV_0) and the increase in the response is given by MEV_1 (Table 5). The cumulative exposure changes based on the difference in *V. tapetis* growth and temperature-dependent death rate (MTV) as

$$\frac{d}{dt}MEV = V - MTV \quad (32)$$

where MTV is the threshold concentration of *V. tapetis* at which exposure accumulates (Table 5). The above formulation allows a cumulative exposure that occurs once the pathogen concentration exceeds a threshold value, thereby introducing a time delay on mortality. The mortality rate increases to a maximum value with sufficient exposure. Exposures to *V. tapetis* concentrations that produce mortality rates below the threshold rate result in a decreased mortality rate.

The mortality resulting from the severity of the BRD symptom (MS) was assumed to follow a similar relationship:

$$MS(t, BRD) = \frac{MS_o}{2}\left[1 + tanh\left(\frac{MES(BRD, t) - MES_o}{MES_1}\right)\right] \quad (33)$$

where the base mortality rate, MS_0, is set to have a halving time of 30 days (Table 5). This response becomes active at a threshold (MES_0) and the increase in the response is given by MES_1 (Table 5). The increase in mortality due to the BRD deposit (MES) is calculated as

$$\frac{d}{dt}MES = BRD - MTS \quad (34)$$

where MTS is the threshold for BRD symptom at which exposure accumulates (Table 5).

Table 5
Units, definitions and values of parameters and coefficients used in the equations that describe clam mortality. CDS = Conchiolin Deposit Stage. See Eqs. (31)–(36) in the text.

Parameter	Units	Definition	Value
MV_0	d^{-1}	Clam mortality rate due to V. tapetis density	0.01155
MEV_0	No units	Coefficient that provides a threshold for the mortality effect due to V. tapetis exposure	120
MEV_1	No units	Coefficient that determines how rapidly clam mortality increases above the threshold response	40
MTV	Cells mL^{-1}	Threshold V. tapetis concentration at which exposure accumulates	5×10^5
MS_0	d^{-1}	Clam mortality rate due to conchiolin deposit	0.0231
MES_0	No units	Coefficient that provides a threshold for the mortality effect due to CDS severity	200
MES_1	No units	Coefficient that determines how rapidly clam mortality increases above the BRD symptom severity threshold	7
MTS	No units	Threshold CDS at which exposure accumulates	3.5
MC_0	d^{-1}	Clam mortality rate due to low condition index	0.0154
MEC_0	No units	Coefficient that provides a threshold for the mortality effect due to clam condition	10
MEC_1	No units	Coefficient that determines how rapidly clam mortality increases above the clam condition threshold	1
MTC	No units	Threshold clam condition at which exposure accumulates	-0.5
MN	d^{-1}	Background clam mortality rate	4.4574×10^{-4}

Clam mortality due to low condition index (MC) was obtained similarly as

$$MC(t,C) = \frac{MC_o}{2}\left[1 + tanh\left(\frac{MEC(C,t) - MEC_o}{MEC_1}\right)\right] \qquad (35)$$

where MC_o is defined with a halving time of 45 days (Table 5). This response becomes active at a threshold (MEC_0) and increases as given by MEC_1 (Table 5). The change in mortality rate as condition decreases or increases (MEC) is calculated from

$$\frac{d}{dt}MEC = -C + MTC \qquad (36)$$

where MTC is the threshold for condition at which exposure beings to accumulate (Table 5). For this mortality response, negative condition results in accumulation of damage.

The natural, or background, mortality (MN), which is independent of phenotype (see Section 6), was set at a constant rate (Table 5) that removes 15% of the clams each year (Hoenig, 1983).

5.4. Transmission

Transmission of V. tapetis to new recruits and other uninfected individuals was assumed to depend on the weighted infection intensity (II) of the clam population, the total clam density (CD), and V. tapetis density in the total population (SV). The time-dependent population-weighted infection intensity was calculated from the change in the severity of the BRD deposit and the V. tapetis density, $WN(t)$, in the total alive portion ($Alive_i(t)$) of the clam population as

$$IIt = \frac{0.5WN(t)}{\sum_{i=1}^{N} Alive_i(t)} \qquad (37)$$

where the subscript, i, indicates an individual simulation of a clam with a particular phenotype. The weighted number of clams was calculated as

$$WN(t) = \sum_i Alive_i(t)(wBRD(BRD_i(t)) + wVib(V_i(t))) \qquad (38)$$

where the weights (wBRD) and (wVib) determine the level of BRD and V. tapetis at which there is a significant contribution to disease prevalence in the clam population. The infectious elements are present in the infected clams and the environment and both need to be included to calculate population disease prevalence. The

level at which BRD and V. tapetis contribute to population infections is calculated as

$$wBRD(BRD) = 0.5\left(1 + tanh\left(\frac{BRD - TEB_0}{TEB_1}\right)\right) \qquad (39)$$

$$wVib(V) = 0.5\left(1 + tanh\left(\frac{log_{10}\left(10^{-6}V\right) - TEV_0}{TEV_1}\right)\right). \qquad (40)$$

The wBRD equation specifies that the BRD stage has to be above CDS 3, and V. tapetis has to be present in concentrations in excess of 3×10^6 cells, to affect to the population prevalence. The V. tapetis weighting equation is constrained so that the $log_{10}V$ is greater than zero. Coefficient values are given in Table 6.

The dependence of transmission on V. tapetis density is obtained by calculating a weighted sum of V. tapetis (SC) as

$$SC(t) = \sum_i Alive_i(t)wBRD(BRD_i(t))wVib(V_i(t)))V_i(t)VPF \qquad (41)$$

where $VPF = 0.7084\,L^{1.956}$ is the estimated volume of the extrapallial fluid in μL for a clam of length L in mm.

An estimate of the amount of infectious agent in the population ($SV(t)$) was obtained by scaling the total number of V. tapetis cells ($SC(t)$, Eq. (41)) by the clam population disease prevalence ($WN(t)$, Eq. (38)) as

$$SV(t) = \frac{2SC(t)}{WN(t)} \qquad (42)$$

which provides an estimate of the amount of infectious agent in the population. The transmission fraction (TF), which is the portion of the total clam population that will become infected, is then calculated assuming a hyperbolic dependence on scaled V. tapetis (SV) and clam density (CD) as

$$TR(II, SV, CD) = \frac{II\,SV}{\frac{0.001 + 5}{CD + SV}} \qquad (43)$$

where the first two terms in the denominator represent the clam density at which the transmission factor is at one-half its maximal rate (the half saturation value for the transmission factor). The coefficient TrF_0 (Table 6) is the transmission factor half saturation value at large CD. For large CD and SV greater than 0.001, transmission is at the maximum rate given by II. In this case, transmission of BRD depends only on how

11

Table 6
Units, definitions and values of parameters and coefficients used in the equations that describe BRD transmission. CDS = Conchiolin Deposit Stage. See Eqs. (37)–(43) in the text.

Parameter	Units	Definitions	Value
TEB_0	No units	Coefficient that provides a threshold for the transmission effect in response to CDS level	3
TEB_1	No units	Coefficient that determines how rapidly transmission increases above the CDS threshold	0.66
TEV_0	No units	Coefficient that provides a threshold for the transmission effect in response to *V. tapetis* concentration	0.5
TEV_1	No units	Coefficient that determines how rapidly transmission increases above the *V. tapetis* threshold concentration	0.33
TrF_0	No units	High clam density half saturation value for infection	0.001
TrF_1	Clams m^{-2}	Coefficient that adjusts the half saturation value for clam density	5

sick the clams are because the density is sufficient to provide proximity to diseased individuals. For small *CD*, the half saturation value for the transmission factor is the sum of the first two terms in the denominator of Eq. (43), which requires that *SV* increases to reach maximum infection rates. Thus, the number of infective particles, as well as the number of sick clams, determines BRD transmission. If clam densities are sufficiently small, it is possible that some individuals will not become infected. The transmission fraction and the number of uninfected clams remaining in the cohort are used to calculate the number of clams that will become newly infected.

6. Model implementation

6.1. Environmental forcing

Environmental effects were included in the model by inputting a time series of temperature and food as external forcing functions. Chlorophyll *a* concentrations measured in the Bay of Brest, northern
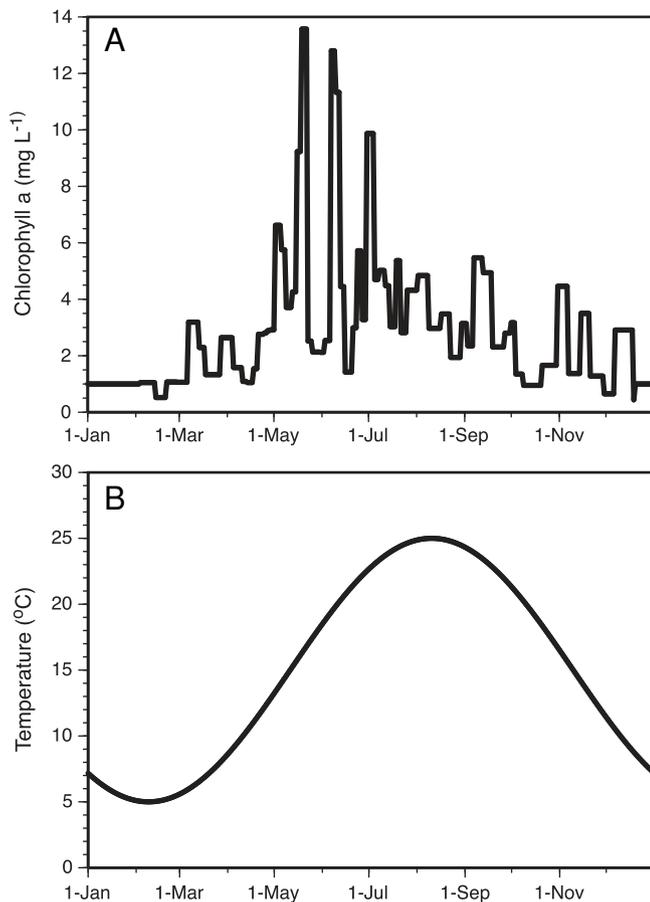

Fig. 11. Chlorophyll a and water temperature values used to construct base-case simulations in Figs. 12 and 13. A. Chlorophyll a values from the Bay of Brest, northern Brittany, France, used to create a food time series for the model. B. Sinusoidal curve representing a one-year temperature time series constructed from two years of partial data from the Gulf of Morbihan, southern Brittany, France.

Brittany, France (Fig. 11A), were used to estimate food concentration (*F*) from a linear regression of the form

$$F = \alpha \times \text{Chla} + \beta \tag{44}$$

where the constants α (0.176 mg μg^{-1}) and β (0.06 mg L^{-1}) convert chlorophyll *a* into non-chlorophyll food (Powell et al., 1997; Soniat et al., 1999).

Limited temperature observations from Landeda and the Gulf of Morbihan, northern and southern Brittany, France, respectively (Laruelle, 1999; Paillard, 1992; Soudant et al., 2004) provided values for the temperature minima and maxima and the timing of the winter minimum temperature. These characteristics were used to construct a year-long temperature time series, assuming that the temperature variation in the Gulf of Morbihan can be described by a sinusoidal dependence. The resultant temperature time series (Fig. 11B) ranges from a low of about 5 °C in January and February to a maximum of about 25 °C in summer.

Although laboratory experiments have shown that BRD is more likely to develop at salinities of 20 to 30, than at 40 (Reid et al., 2003), neither salinity nor total suspended solids were included as environmental forcing functions in the BRD model as most locations in Western Europe where the Manila clam grows are characterized by relatively clear waters and relatively invariant salinity of 30–35 (Laruelle, 1999; Paillard, 1992).

6.2. Simulation scenarios

The BRD model was implemented with the parameter and coefficient values given in Tables 1, and 3–6 and the temperature time series shown in Fig. 11B to establish a reference simulation, which is described in Section 8. This simulation provides a basis for comparison with simulations obtained with different processes, parameter values, or environmental forcing.

The observations of BRD in cultured and wild clam populations (Fig. 1) showed differences in the pattern of disease progression over a year. An implication of these observations is that the characteristics of BRD disease differ in the two populations. One possible explanation for this difference is that wild clam populations are more fit than those in culture and are therefore better able to counteract the effects of BRD. To test this, simulations were done in which the assimilation and hemocyte activity rates were increased to 1.2 (120% of the base rate, see Section 6.1), which gives the clams improved condition and ability to eliminate *V. tapetis*. A second set of simulations considered possible effects of changing temperature regimes, as might occur with climate warming, on BRD prevalence and intensity. For these simulations, the input temperature time series (Fig. 11B) was modified by 1) increasing the temperature by 2 °C over the entire year, 2) increasing the winter (November to March) temperatures by 1 °C and 2 °C, and 3) increasing the summer (May to September) temperatures by 1 °C and 2 °C.

6.3. Numerical integration

The set of first-order ordinary differential equations that make up the BRD model (Eq. (9)) were solved numerically using a compact fourth-order Runge–Kutta time integration routine. The time interval

used for the simulation was one day, which is sufficient to resolve the model processes.

The simulations were run for three years. The first year allows for the clam and BRD biological processes to adjust to one another and for the clam and disease to adjust to the environmental conditions. The second and third simulation years are used for analysis.

7. Results

7.1. Simulated time-development of BRD

The observed distribution (Fig. 12A) of BRD stages in clams experimentally deployed in June in the Gulf of Morbihan, southern Brittany, France provided the basis for evaluating the realism of the distributions obtained from the BRD reference simulation. The observations showed patterns and levels typical of cultured clams (Fig. 1A). A brief peak of moderate stages (CDS 3) occurred in early summer representing clams infected in late spring, and a major peak of both moderate and heavy stages developed during the fall, reaching maximum levels in winter. The rapid decline in summer is due to repair and recovery of some individuals and the death of others that were unable to effectively combat *V. tapetis*.

The simulated time-development of BRD (Fig. 12B) shows a rapid increase in the severity of the symptom during the summer, a prolonged peak in fall and winter, followed by a decrease the following spring and early summer. The timing of increases and decreases in BRD in the simulated clams agrees with observations. However, the overall intensity of
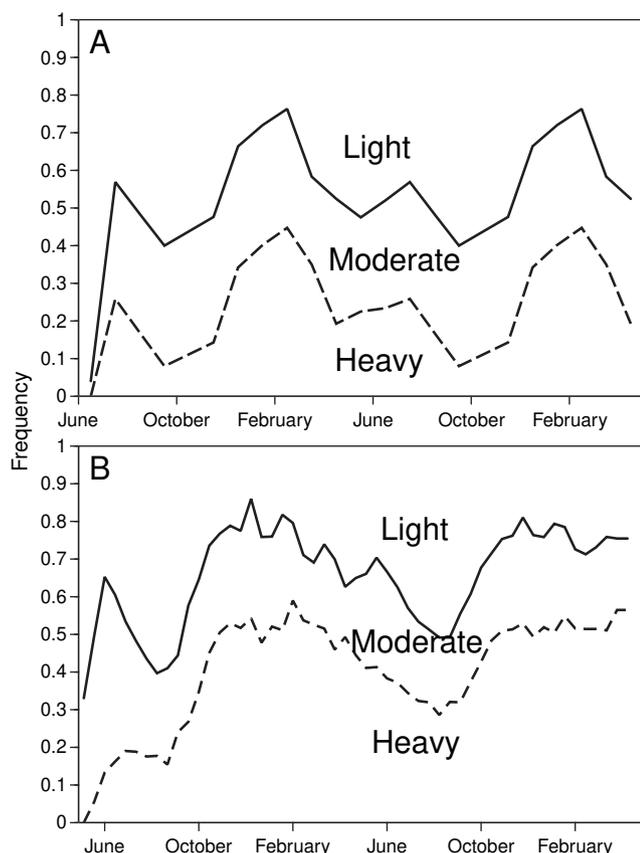

Fig. 12. Observed A. and simulated B. seasonal distribution of Brown Ring Disease groups among affected clam cohorts. Observed data were obtained from clams deployed in the Gulf of Morbihan, southern Brittany, France. Note that a single season's observed data are plotted twice. The simulation covers two years after an infection period in June, July and August of year one during which one third of the cohort was infected each month. Light = CDS 1 & 2; moderate = CDS 3; heavy = CDS 4–7.
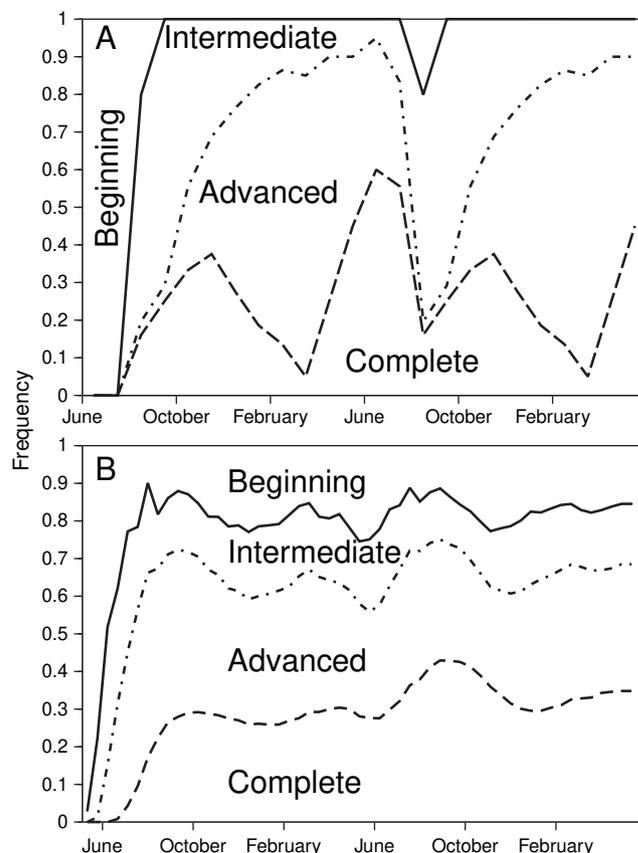

Fig. 13. Observed A. and simulated B. seasonal patterns of Shell Repair Stage in Brown Ring Disease among affected clam cohorts. Observed data were obtained from clams deployed in the Gulf of Morbihan, southern Brittany, France. Note that a single season's observed data are plotted twice. The simulation covers two years after an infection period in June, July and August of year one during which one third of the cohort was infected each month. Beginning = SRS 1; intermediate = SRS 2; advanced = SRS 2.5; complete = SRS 3.

BRD levels in the simulation is higher than observed for the clams in the Gulf of Morbihan.

The observed SRS (Fig. 13A) indicates that clams rapidly begin to cover the BRD deposit. Most affected clams have passed through the first two stages (1 and 2) and into stage 2.5 or 3 during the late summer and fall. A decline in the fraction of clams in stage 3 during the winter is followed by a rapid increase as the temperature warms in spring. By May and June, most affected individuals have either completely or nearly completely covered the deposit.

The simulated time development of SRS (Fig. 13B) also shows a rapid increase in repair with most individuals being in stages 2.5 or 3 by late summer. However, the simulated SRS stages have fewer clams in intermediate and advanced stages relative to observations, especially in winter and spring, and more remain in the beginning SRS stage. Also, the variation in stage 3 seen in the field observations is not reproduced in the simulation.

The simulated cumulative mortality (Fig. 14) provides a measure of the relative effect of the different components of mortality in producing the patterns in BRD development. For the reference simulation, most of the clam mortality is from the effects of *V. tapetis*. Mortality resulting from BRD deposits is about half of that caused by *V. tapetis*. Low condition accounts for a relatively constant low-level source of mortality.

7.2. Simulations of conceptual model for different phenotypes

Over a 4 year period post-infection, the behavior of the simulated population is best understood by looking at sub-groups of the population having different physiological capabilities represented by the
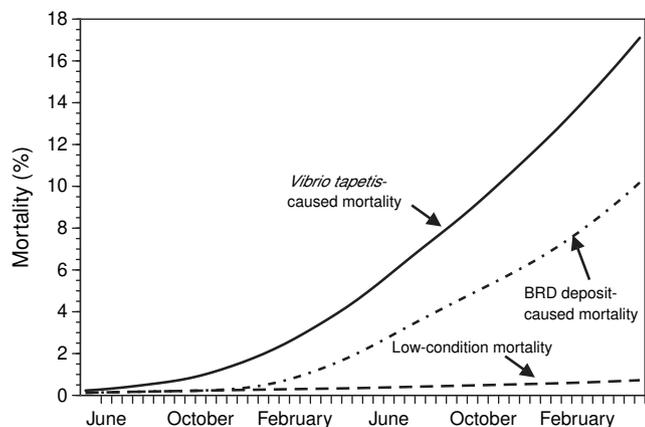
Fig. 14. Simulated clam mortality showing the relative contribution of the different non-background causes of death in a clam cohort. Background mortality is a constant 15% per year and, if plotted, would not change the pattern of the other sources.

different phenotypes (Fig. 15A–C). Simulated disease trajectories show that clams with the highest assimilation (ASSIM), calcification (CAL) and hemocyte (HC) activity rates (i.e., HHH) reduce bacterial density and begin shell repair almost immediately after infection and never progress much beyond CDS 2 (Fig. 15A). Repair is rapid and complete (SRS 3), and the clams return to CDS 0 in year 2. But not all *V. tapetis* are eliminated and a second and then third episode of bacterial proliferation occurs. Repair continues to be rapid and complete after each episode. For clams representing intermediate levels of each process (III), repair begins much more slowly and the CDS reaches 4 during year 1 (Fig. 15B). But repair is completed in year 2. After subsequent re-proliferation episodes, repair begins much more rapidly than in year 1, although CDS 4 is reached briefly in years 3 and 4. Individuals with the lowest rates (LLL) progress through increasingly severe brown ring stages toward CDS 7 with no evidence of repair (Fig. 15C). It should be noted that these trajectories do not consider mortality, so the individual with phenotype LLL may die before the trajectory is completed. BRD-associated mortality is a function of condition index and *V. tapetis* density, as well as CDS, and the exposure time to each of these conditions. Thus, the chance of mortality increases as the disease progresses.

By holding each of the three parameters at the highest or lowest phenotypes, and varying the levels of the other two parameters, it is possible to simulate the relative importance of each parameter and its phenotypes in individual clam trajectory plots (Fig. 16). Noteworthy is the observation that an individual with the highest phenotype in one parameter and the lowest phenotype in the other two will inevitably move along the death trajectory toward CDS 7 (Fig. 16A, C, E). The specific parameter having the highest phenotype, however, alters the trajectory. For instance, although two low phenotypes eventually lead to CDS 7, individuals with the highest assimilation (Fig. 16A) show some evidence of repair, whereas those with the highest hemocyte activity or highest calcification rates show none. A more marked illustration of the effect of phenotype is observed when the lowest phenotype of one parameter is combined with varying phenotypes of the other two. When either assimilation or hemocyte activity is low, the individual shows no evidence of repair, regardless of the level of the other parameters (Fig. 16B, F). In contrast, an individual with low calcification, but high assimilation and hemocyte activity repairs rapidly and completely each time bacterial proliferation commences (Fig. 16D). Even when assimilation and hemocyte activity are intermediate and calcification is low, shell repair is initiated, although never completed, before the individual reaches CDS 7. It should be noted that the downward loops in Fig. 16A and D are artifacts of the model that occur after the clam would have died.
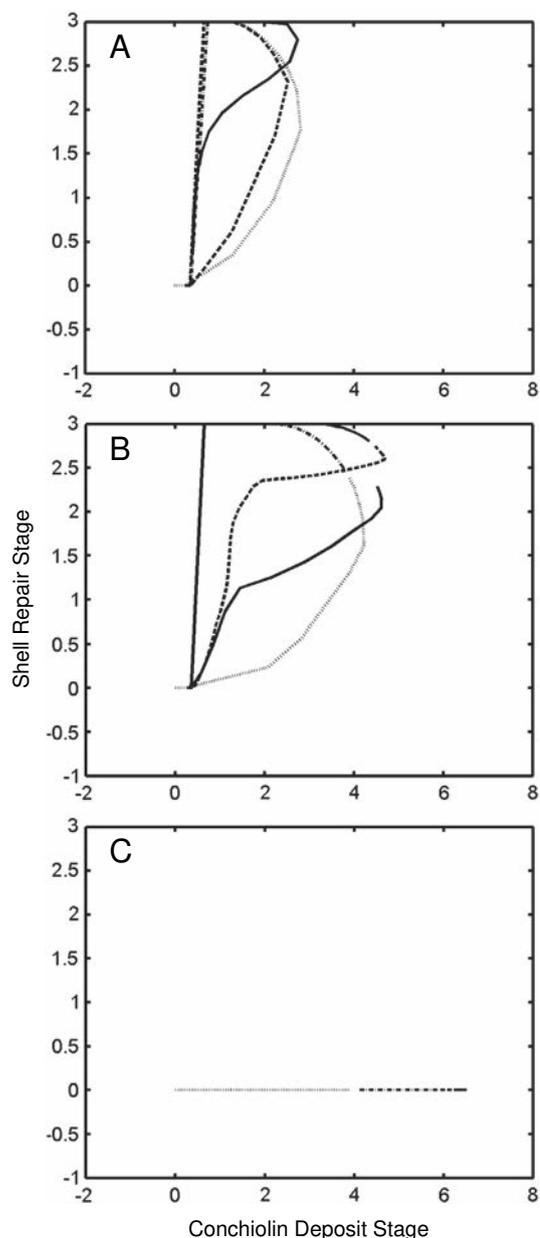

Fig. 15. Simulated trajectories for A. a clam with the best assimilation, $CaCO_3$ deposition and hemocyte responses; B. a clam with intermediate rates; and C. a clam with the lowest rates. The simulations cover four years after a July infection period. Year 1 = ..., year 2 = _ . _ ., year 3 = _ _ ., and year 4 = ——.

7.3. Contribution of physiological parameters to individual performance

The physiological relationships in the model help explain the disease/recovery trajectories and the relative importance of the parameters in Fig. 16. The model varies relationships of the three physiological parameters according to phenotype. For instance, the food assimilated by a clam is linearly related to the concentration of food in the water, but depends also on the assimilation capacity or phenotype of that individual (Fig. 17A). The best phenotype (180% of mean) takes maximum advantage of increases in food availability. At 1 mg L^{-1} of available food, these individuals can assimilate about 20 mg day^{-1}. At 2.5 mg L^{-1}, they can assimilate more than 50 mg day^{-1}. At the same food concentrations, the worst performers (20% of mean) assimilated only 2 and 5 mg day^{-1}, respectively. Although, the relative difference between phenotypes remains constant, the absolute difference
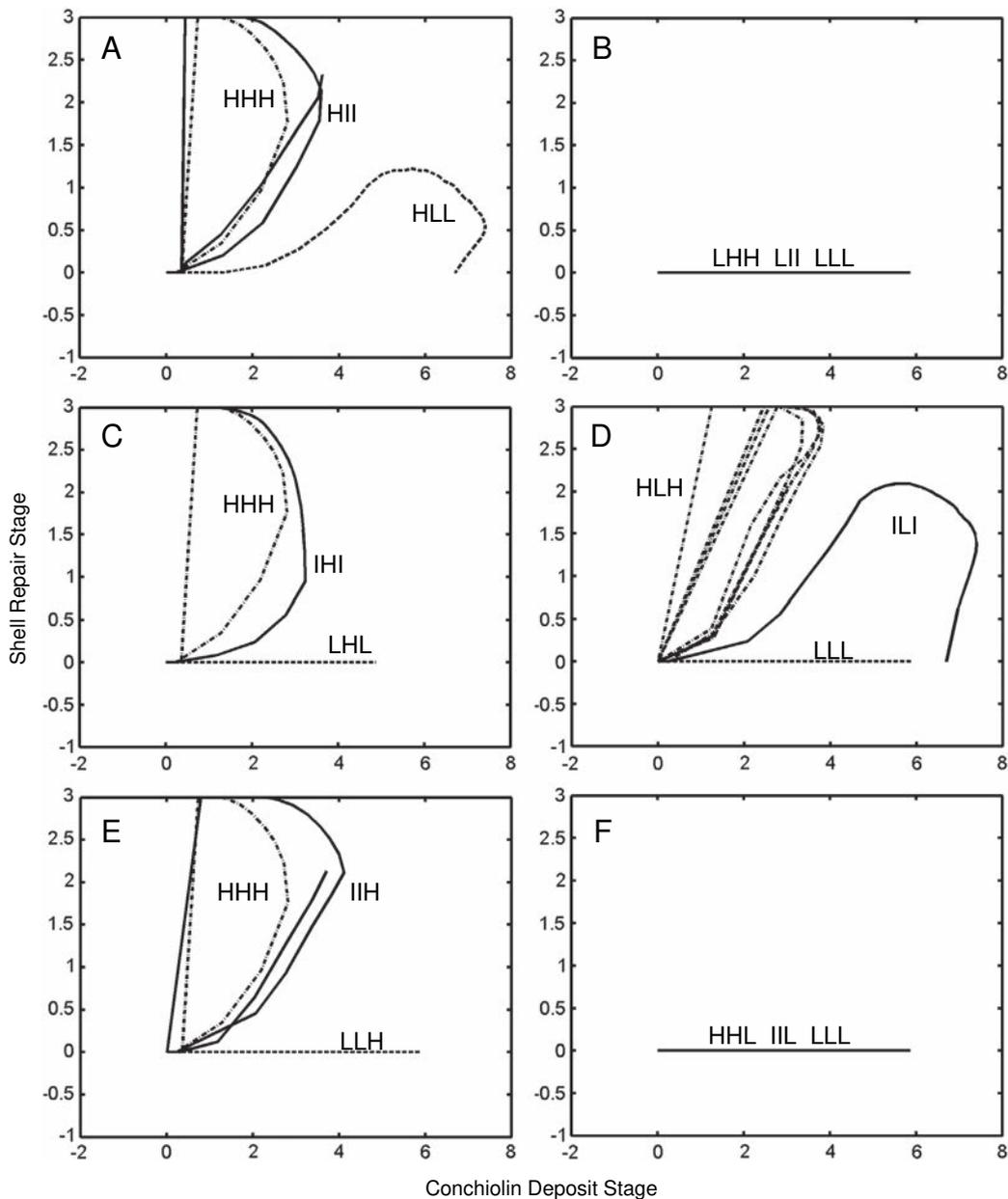
14

Fig. 16. Simulated trajectories for individual phenotypes showing the relative importance of A. and B. Assimilation activity; C. and D. CaCO₃ deposition, and E. and F. hemocyte activity in the model. In each figure, the three lines represent an individual of a unique phenotype labeled by a 3-letter code. The first letter of each code represents the assimilation rate, the second, the CaCO₃ deposition rate, and the third, the hemocyte activity. H = high; I = intermediate; L = low. (A & B) Relative importance of assimilation (ASSIM). A. high ASSIM; HC and CAL, varied similarly. B. low ASSIM; HC and CAL varied similarly. (C & D) Relative importance of calcification (CAL). C. high CAL HC and ASSIM varied similarly. D. low CAL, HC and ASSIM varied similarly. (E & F) Relative importance of hemocyte response (HC). E. high HC, ASSIM and CAL varied similarly. F. low HC, ASSIM and CAL varied similarly.

increases constantly as food supply increases. Thus, the best performers are able to take increasingly greater advantage of greater food availability, such as that used in the model (Fig. 11A) and high assimilation can compensate for low calcification and phagocytic rates.

Shell repair is positively related to the amount of conchiolin in the brown ring deposit and to the relative ability of clams to produce CaCO₃ (Fig. 17B). By the time conchiolin weight reaches about 0.015 g (CDS between 5 and 6), the best performers can deposit about 5 mg CaCO₃ day⁻¹, whereas the worst can deposit only about 0.5 mg day⁻¹. The rate of increase in deposition slows markedly, even for the most proficient individuals, as the amount of conchiolin increases. At the highest simulated conchiolin weight (0.04 g), the best performers have added only 2 mg day⁻¹ to their deposition rate.

Thus, CaCO₃ deposition rates are not as sensitive to changes in an influencing variable as is assimilation and do not favor the best performers as much; hence, high calcification cannot compensate for low assimilation or phagocytosis.

Condition index (CI) is inversely related to the halving time (and thus inversely to the proliferation rate) of *V. tapetis* (Fig. 17C). This relationship operates through the direct relationship between CI and hemocyte density, which in turn raises the number of phagocytes capable of ingesting and killing bacteria as the CI increases. At high CI (0.5), all phenotypes can maintain halving time at a day or less, but as CI decreases, the low performers lose this ability much more rapidly than the high performers. At a low CI (−1), the worst performers take 9 days to reduce the bacterial concentration by half, whereas the best performers take only one day.
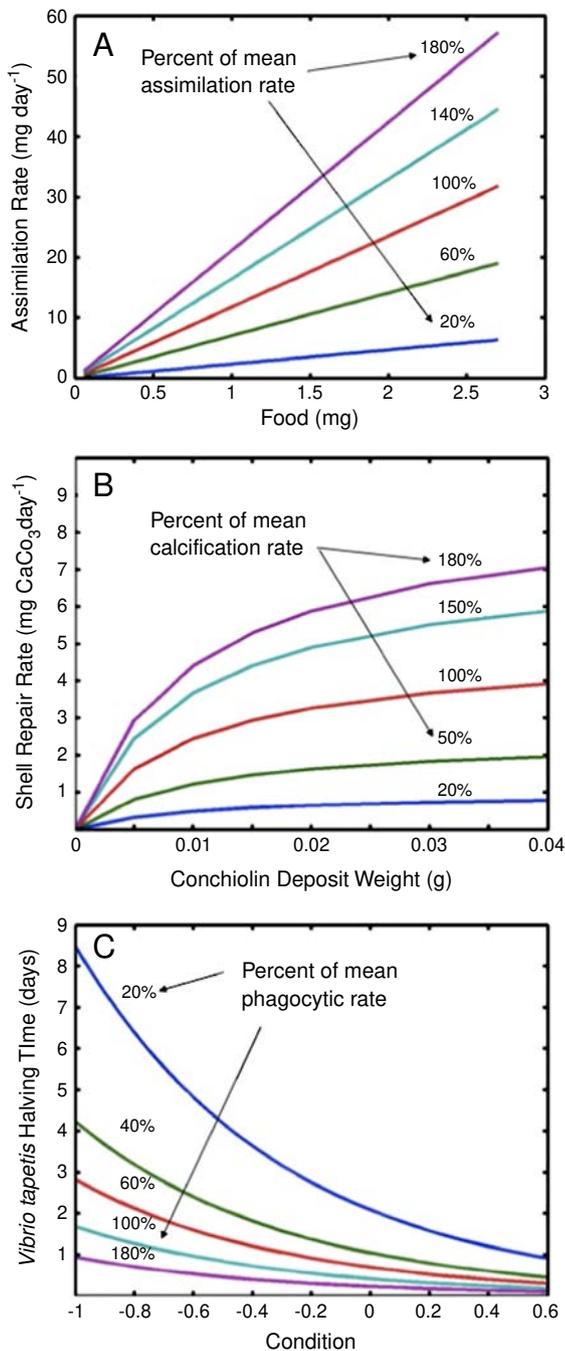
Fig. 17. Model relationships showing how phenotype influences physiological rates: A. Assimilation rate vs available food varied by assimilation capacity; B. Shell repair rate vs conchiolin deposition varied by $CaCO_3$ deposition capacity; C. *Vibrio tapetis* halving time (death rate) vs condition index varied by hemocyte activity.

7.4. Variation of temperature

The altered temperature scenarios (simulations not shown) did not show any obvious changes in the seasonal patterns of CDS and SRS relative to the reference simulations (Figs. 12 and 13). However, more subtle changes produced by the altered temperature scenarios were investigated by calculating deviations from the reference simulation frequency distributions (Fig. 18). For most of the scenarios, the seasonal deviation patterns are similar and the CDS deviations (Fig. 18A–E) are opposite of the SRS deviations (Fig. 18F–J). The magnitude of the deviations varies according to time post-infection as well as with the simulated temperature regime.

For the CDS simulations, most of the deviations are positive, ranging up to 0.2 units (i.e., a 20% increase in the frequency of both moderate and heavy stages over the reference simulation), with maxima in winter to mid-summer and minima in the fall (Fig. 18A–E). In two simulations (2 °C increase year round and 1 °C increase in November–March), the deviations became negative in the fall, declining by −0.4 units in the first year. In addition to having substantial negative deviations, the simulation with the smallest positive deviation was for the 1 °C increase in November–March (Fig. 18B).

Deviations for SRS from the reference simulation were almost entirely negative for all simulations (Fig. 18F–J). Pronounced decreases were associated with all stages, but especially the intermediate stage during the spring and summer of the first year, which declined to −0.4 to −0.5 in all but the simulation that used a uniform 2 °C increase. In this scenario, intermediate stage deviations were steadily negative for most of the two-year simulation. The advanced and complete stage deviations varied seasonally, becoming slightly positive in the winter, especially of the second year, when intermediate stage deviations from the negative became less pronounced (Fig. 18F). In all the other SRS simulations, the complete stage deviation remained consistently negative until the second winter, whereas the other two stages showed a more seasonal pattern, becoming less negative, and even slightly positive, in the fall before rapidly becoming negative again in the winter. With the exception of the steep negative deviations in the first year, SRS deviations ranged between −0.2 to +0.1.

7.5. Variations of clam assimilation efficiency and hemocyte activity

As expected, increasing assimilation efficiency and hemocyte activity by 120% decreased the frequency of all CDSs and increased the frequency of SRSs; however, these changes were half or less (ranging from −0.1 to +0.1 units for assimilation and –0.05 to +0.03 for hemocyte activity) than those simulated for the increased temperature regimes (simulations not shown).

8. Discussion

Evaluation of the BRD model was provided by assessing the ability of the simulated distributions to reproduce the seasonal cycle of the two primary disease indices, CDS (conchiolin deposit stage) and SRS (shell repair stage), including timing and amplitude of peaks in these indices for cultured clams. The heaviest observed conchiolin deposits occur in the winter and early spring, and they decline in late spring and summer. The fraction of CDS categorized as moderate or heavy peaks at about 80%. Simulated disease stages follow a similar pattern, with peaks in the winter and spring and low disease levels in summer. The frequency of disease stages in the simulations was also similar to the observed frequencies. Thus, at a population level, the model is able to simulate field observations of CDS frequency. The simulation of the seasonal variation in shell repair stages, however, was not in as good of agreement with observations. Specifically, the model produced a substantial number of beginning repair stages that were not observed in the field, and did not show the large seasonal variations that were observed in the field. Shell repair is the result of several factors that include animal condition, the amount of conchiolin present and bacterial density. The approach used to link these factors to initiate and maintain shell repair is based on limited empirical data and assumptions about the relationships between $CaCO_3$ and conchiolin deposition, host assimilation, and hemocyte activity. Although these relationships are based on current understanding, the inability of the model to accurately simulate shell repair suggests that a critical process(es) is missing. The nature of this process is unknown, but may be related to the rate of shell repair once initiated. In fact, Trinkler et al. (2010a) have shown that the shell repair layers could reach an average a thickness of 800 μm, containing a progressive
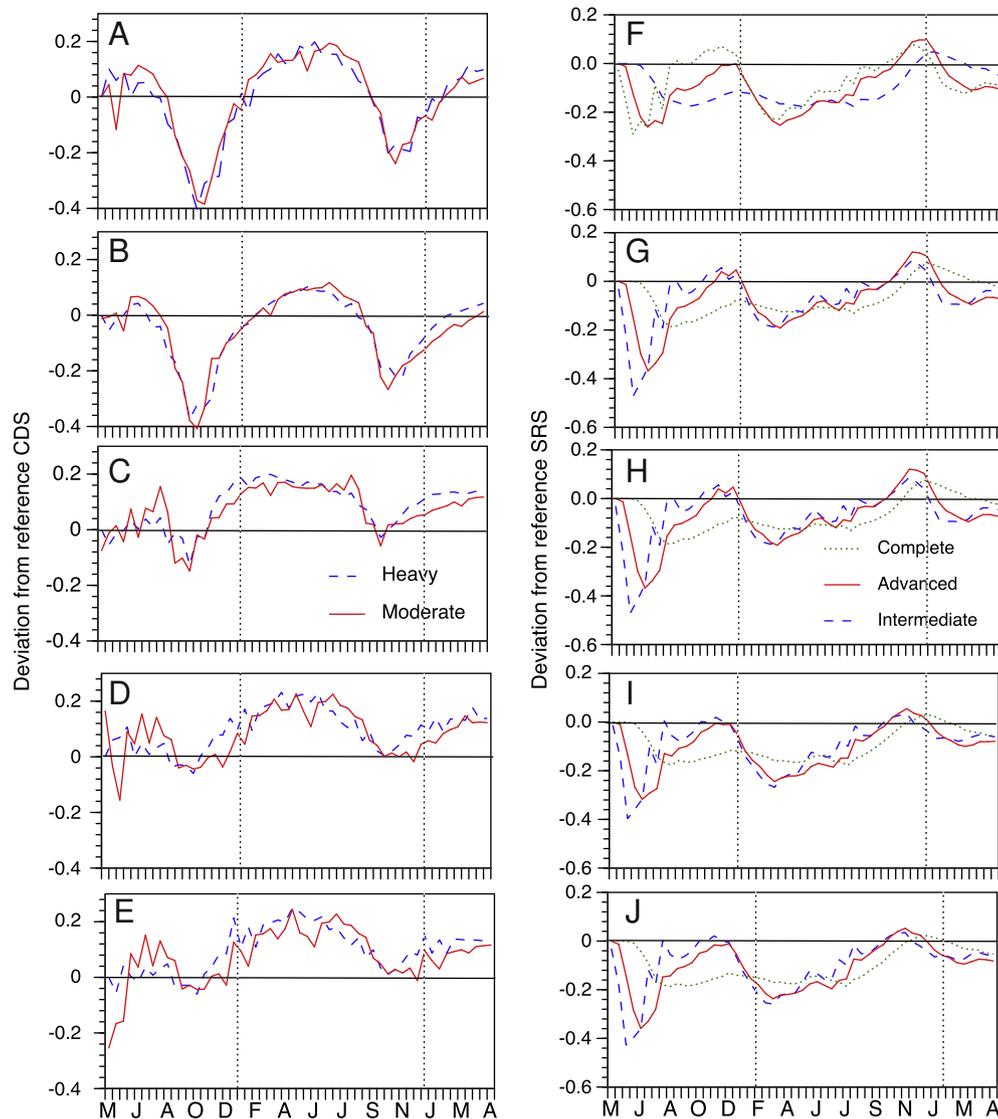
Fig. 18. Simulated deviations from the base case over a 2-year cycle under several temperature warming scenarios for a single clam cohort. A–E: CDS (Conchiolin Deposit Stage); F–J: SRS (Shell Repair Stage). Reference simulations are shown in Fig. 12 for CDS and Fig. 13 for SRS. A & F. 2 °C temperature increase in each month of the year; B & G. 1 °C increase in winter months (November-March); C & H. 2 °C increase in winter months (November–March); D & I. 1 °C increase in summer months (May–September); E & J. 2 °C increase in summer months (May–September). Deviation units represent the difference in the frequency of each stage between the base case and the altered scenario.

decrease of conchiolin, before being detected as a non-BRD affected inner layer. Clearly this is an area for further study.

Populations are collections of individuals with different genotypes and phenotypes, which can result in disparate outcomes when a disease agent challenges those individuals. The coupled BRD-Manila clam model is unique among disease models in that it tracks the behavior of individuals. The trajectories described for individual clams show how different phenotypic values of the three model parameters – assimilation, calcification, and hemocyte response – result in vastly different outcomes from an infection by *V. tapetis*, the agent of BRD. The model provides a theoretical framework primarily because it is individually based and it is not presently possible to validate the individual results with observed data on genotype, physiological phenotype, or the disease and repair processes. In fact, attempts to follow disease in individual molluscs by repeated sampling may alter the disease being measured (Ford, 1986; Ford and Paillard, 2007; Malham et al., 1998). Nevertheless, the ability to model individuals within a population has many advantages. For instance, Flye-Sainte-Marie et al. (2007a) illustrated how variations in the timing of spawning of individual Manila clams could confound the interpretation of temporal changes in mean population weight. This study showed that mean population

trajectories are not the same as the trajectory of the "mean" individual and the "mean" individual does not necessarily represent the population mean.

Simulation of the disease and repair trajectories of individual clams permitted investigation of the relative importance of assimilation, calcification and hemocyte response in the outcome of the host–parasite interaction. Varying the phenotypes helps to understand the complex interactions among the model processes in producing disease and recovery. Individuals with the highest assimilation phenotype initiate shell repair and delay mortality even when the phenotypes of the other two parameters are low. The same is not true of individuals with the best calcification or hemocyte response if assimilation is low; they do not even begin repair. A similar outcome was evidenced by simulating CDS and SRS of a single cohort of clams having 120% of the base assimilation efficiency or 120% of the base hemocyte activity. In the first case, CDS decreased by a maximum of 10% and SRS increased by a similar amount, whereas when hemocyte activity was increased, the maximum decrease in CDS was 5% and the maximum increase in SRS was only 3%.

Simulations indicate that high or intermediate assimilation or hemocyte response can rescue an individual with low calcification from rapid

death, whereas low assimilation or hemocyte activity results in increasingly severe disease and eventual death regardless of the phenotypes of the other parameters. Low assimilation or hemocyte response leads to death, with no evidence of repair, even when the other phenotypes are high. Of the three modeled phenotypes, therefore, assimilation plays the greatest role in the outcome of the disease process, and calcification, the least important role. Assimilation capacity is the dominant process because until BRD becomes severe, it is affected almost entirely by the environmental variables food and temperature. Only at CDS 5, is assimilation capacity significantly impaired when the conchiolin deposit begins to interfere with filtration. In contrast, calcification for shell repair plays a secondary role, being entirely dependent on the presence and abundance of conchiolin, which in turn is a function of *V. tapetis* density. Bacterial density itself is affected by a chain of parameters including hemocyte response, condition, food and temperature. Hemocyte response is intermediate in importance, in that it is a function of bacterial density and condition, the latter being affected by assimilation. Individuals with high hemocyte-response phenotypes behave like those with high calcification phenotypes, recovering more slowly than those with high assimilation capacity; individuals with low hemocyte phenotypes behave like those with low assimilation phenotypes, evidencing no repair.

Although the results of individual trajectories cannot be validated for the reasons discussed above, the parameter values for assimilation, calcification, and hemocyte response were obtained from experimentally derived or observed data and are considered reasonable estimates of the physiological rates involved. Some factors were estimated, including the effect of BRD on filtration rates of affected clams, which in turn affects assimilation and energy availability. The filtration parameterization used in the model assumes that filtration rate begins to decline at about CDS 2.5, but is not severely reduced until CDS 5. By CDS 7, the rate is about half of that of unaffected clams. Recent laboratory measurements of clams in various stages of BRD (Flye-Sainte-Marie et al., 2007b) indicate that the measured effect begins at CDS 4 and decreases by about 67% at CDS 7. Thus, the model filtration rate probably underestimates the effect of advanced BRD, although the rate falls within the range of individual measurements made by Flye-Sainte-Marie et al. (2007b). The baseline filtration rate for unaffected clams relies on measurements (Goulletquer, 1989; Goulletquer et al., 1989), and is similar to those measured by Flye-Sainte-Marie et al. (2007b). In addition, rates lower than those frequently measured in the laboratory are likely to occur in nature (Powell et al., 1992; Riisgard, 2001). A recent estimate of the energetic costs of BRD, based on Dynamic Energy Budget (DEB) methodology (Flye-Sainte-Marie et al., 2009a), suggests that in addition to the feeding interference posed by the conchiolin deposit, maintenance metabolism increases substantially during infection, thus further affecting the energy balance of diseased clams.

Other parameterizations used in the model are based on assumptions about how processes operate rather than on empirical evidence. For example, the BRD model initiates an infection with a single pathogen, which leads to an interesting and unexpected problem that may be biologically relevant. The number of phagocytically capable hemocytes in the extrapallial cavity, where bacteria initially lodge (Allam et al., 1996; Paillard and Maes, 1995b), is large relative to the simulated infectious dose. Thus, initial simulations failed to establish an infection because all invading bacteria were immediately ingested. To allow bacteria to become established, a lag time between bacterial invasion and the hemocyte response was included so that the bacterial population could expand to a point at which it is not immediately eliminated by the hemocytes. An implication of this parameterization is that in actuality the bacterium in some way avoids hemocytes during the early stages of infection or that the hemocytes require an interval before they start recognizing and ingesting the invader.

The interaction of clam hemocytes and *V. tapetis* has been studied (Allam and Ford, 2006; Allam et al., 2001, 2006; Choquet et al., 2003). Hemocytes phagocytose the bacteria, but the ability of the clam

cells to kill the ingested bacteria is presently uncertain and some evidence exists that the latter are not killed, at least immediately (Allam et al., 2002b). Recent electronic microscopic observations have shown that *V. tapetis* can survive in hemocytes, at least during 3 days (Paillard and Donval, unpublished data). Further, *V. tapetis* has a toxic effect on clam hemocytes when tested in vitro (Choquet et al., 2003) and the proportion of nonviable hemocytes rises during the development of BRD (Allam et al., 2002a, 2006). Initial "avoidance" might involve failure of hemocytes to kill the bacterium or the toxic effect of the bacterium on hemocytes, although why this would be more effective at low bacterial concentrations than at high is not clear. Alternatively, the delay needed in the simulated disease process may simply be a surrogate for a much larger infective dose, which is probably typical of field exposure. In fact, the lowest dose of *V. tapetis* injected into the mantle cavity of clams found to result in BRD is 10^3 CFU ind^{-1}. Infection by immersion requires on the order of 10^6 CFU mL^{-1} (Drummond et al., 2007; Jean et al., 2011).

An important difference between the BRD model and the earlier oyster disease models (Ford et al., 1999; Hofmann et al., 1995) is that the diagnosis of BRD is based on a symptom, not the presence of a pathogen. Disease severity is scored by the intensity of the symptom and the extent of shell repair, not the number of bacteria. The relationship between *V. tapetis* density in the extrapallial cavity, where the symptom develops, and various measures of BRD showed that this is not a straightforward relationship. Also, in a clam with BRD, conchiolin deposition and CaCO$_3$ layering over the deposit happen concurrently. This requires that the model be capable of describing a trajectory that allows individuals with a given bacterial load to be in different stages of the disease depending on the interaction at any given time between the amount of conchiolin on the shell and the amount of CaCO$_3$ deposited over the conchiolin. Tracking individuals allowed this interaction to be followed in the simulations.

The coupled clam-BRD model can be used to provide a potential explanation for the observed difference between BRD in cultured and wild Manila clams. Cultured clams, on which the model is calibrated, show high BRD prevalence and a clear seasonal pattern (Paillard et al., 1994). Wild clam populations show lower prevalence with no seasonal signal (Flye-Sainte-Marie et al., 2009b). One possible explanation is that handling of clams, as is done under culture conditions, significantly enhances the development of BRD (Jean et al., 2011), a situation that is not included in the model used in this study.

Outbreaks of BRD have been documented primarily in northern Europe, resulting in its designation as a "cold-water" disease; thus the possible impact of climate warming on BRD is of interest. Would increasing temperatures decrease the prevalence of the disease? The BRD model includes temperature as a forcing function, permitting exploration of different warming scenarios. Two of five simulations, involving increases of 1 °C in winter or 2 °C throughout the year (Fig. 18A, B), did show marked reduction in the disease stage (CDS) in the fall, but this is when the severity of BRD is already low (Fig. 12). The severity then increased relative to the reference simulation during the winter and spring, when severity is the highest under current conditions. In the other three simulations, involving increases of 1 °C and 2 °C in summer and 2 °C in winter, severity increased over those obtained from the reference conditions during most of the year. Similarly, the model indicated that shell repair (SRS) would be mostly reduced under all scenarios. Thus, overall, the temperature simulations suggest that the disease would not be constrained by increasing temperatures, and might well be favored. In fact, observation of BRD signs in *V. philippinarum* in waters of southern Spain and Italy (Paillard, 2004b) suggests that high temperatures do not prevent the disease from affecting clams in the field.

The model can also be used to simulate the development of resistance to BRD, which is one of the hypotheses for the low prevalence in the wild clams. Because the phenotypes of simulated individuals are known, their disappearance from the population through BRD-associated mortality can be tracked over time. As the frequency of the

"better" phenotypes begins to predominate, the effects of *V. tapetis* in the population will diminish. The rate at which this happens in a single cohort can be simulated with the present model; however, for a population in which reproduction leads to genetic recombination, a more sophisticated population model with a gene component is needed. A gene-based population model developed for oysters by Powell et al. (2011b) has been used to investigate the development of disease resistance in the eastern oyster, *C. virginica* (Powell et al., 2011a) and to examine metapopulation gene flow (Monroe et al., 2012). This individual-based model simulates genetic changes over multiple generations according to the number of parents involved and their genotypes. Parents are assigned the correct number of chromosomes for the species, with multiple genes on each chromosome and varying numbers of alleles per chromosome. The individual nature of the BRD model allows coupling to the gene model, with the varying capacities assigned to assimilation, calcification and phagocyte activity in the current model being transposed into allelic variation. Other parameters could also be added as genes with alleles that confer different fitness outcomes.

The coupled BRD-Manila clam model provided a framework for synthesizing a considerable amount of information about the BRD process, its effect on the host, and interactions with environmental conditions. The model represented general patterns of the disease progression and provided a basis for qualitative and quantitative comparisons with existing data sets and current understanding. The strength of this modeling approach is that it quantified disease effects, while highlighting uncertainties in data, which is potentially useful for indicating where additional measurements are needed. These range from better definition of temperature effects on rates to new process studies, such as defining the delay between infection initiation and hemocyte response and refining the processes that initiate and produce seasonal variation in shell repair. The model also provides the capability of investigating effects of longer-term environmental changes, particularly increasing temperature, which potentially exerts controls on the prevalence and distribution of BRD. Moreover, the additive effects of temperature and food variability may amplify the effects of BRD in clams, resulting in unanticipated outcomes. Thus, continued refinement of the BRD-clam model and inclusion of an explicit genetics model are the next steps in developing a capability to test scenarios to project the future states of BRD prevalence and distribution, and consequences for Manila clams.

References

Allam, B., Auffret, M., 2000. Induction of an antibacterial activity in the hemolymph of the Manila clam, *Ruditapes philippinarum*. J. Sci. Liban. 1, 3–11.

Allam, B., Ford, S.E., 2006. Effects of the pathogenic *Vibrio tapetis* on defence factors of susceptible and non-susceptible bivalve species: I. Haemocyte changes following in vitro challenge. Fish Shellfish Immunol. 20, 374–383.

Allam, B., Paillard, C., 1998. Defense factors in clam extrapallial fluids. Dis. Aquat. Org. 33, 123–128.

Allam, B., Paillard, C., Maes, P., 1996. Localization of the pathogen *Vibrio* P1 in clams affected by Brown Ring Disease. Dis. Aquat. Org. 27, 149–155.

Allam, B., Paillard, C., Auffret, M., 2000. Alterations in hemolymph and extrapallial fluid parameters in the Manila clam, *Ruditapes philippinarum*, challenged with the pathogen *Vibrio tapetis*. J. Invertebr. Pathol. 76, 63–69.

Allam, B., Ashton-Alcox, K., Ford, S.E., 2001. Hemocyte activities associated with resistance to brown ring disease in *Ruditapes* spp. clams. Dev. Comp. Immunol. 25, 365–375.

Allam, B., Ashton-Alcox, K.A., Ford, S.E., 2002a. Flow cytometric measurement of hemocyte viability and phagocytic activity in the clam *Ruditapes philippinarum*. J. Shellfish Res. 21, 13–19.

Allam, B., Paillard, C., Ford, S.E., 2002b. Pathogenicity of *Vibrio tapetis*, the etiological agent of brown ring disease in clams. Dis. Aquat. Org. 48, 221–231.

Allam, B., Paillard, C., Auffret, M., Ford, S.E., 2006. Effects of the pathogenic *Vibrio tapetis* on defence factors of susceptible and non-susceptible bivalve species: II. Cellular and biochemical changes following in vivo challenge. Fish Shellfish Immunol. 20, 384–397.

Anderson, R.M., 1982. The Population Dynamics of Infectious Diseases: Theory and Applications. Chapman and Hall, London.

Anderson, R.M., May, R.M., 1991. Infectious Diseases of Humans, Dynamics and Control. Oxford University Press, Oxford.

Bailey, N.J.T., 1975. The Mathematical Theory of Infectious Diseases and its Application. Griffin, London.

Blower, S., Roughgarden, J., 1987. Population dynamics and parasitic castration: a mathematical model. Am. Nat. 129, 730–754.

Borrego, J.J., Castro, D., Luque, A., Paillard, C., Maes, P., Garcia, M.T., Ventosa, A., 1996. *Vibrio tapetis* sp. nov., the causative agent of the brown ring disease affecting cultured clams. Int. J. Syst. Bacteriol. 46, 480–484.

Brown, G., 1987. Modeling. In: Fuxa, J.R., Tanada, Y. (Eds.), Epizootiology of Insect Diseases. John Wiley and Sons, New York, pp. 43–68.

Cheng, T.C., 1967. Marine Molluscs as Hosts for Symbioses. Academic Press, New York.

Choquet, G., Soudant, P., Lambert, C., Nicolas, J.L., Paillard, C., 2003. Reduction of adhesion properties of *Ruditapes philippinarum* hemocytes exposed to *Vibrio tapetis*. Dis. Aquat. Org. 57, 109–116.

Drummond, L.C., Balboa, S., Beaz, R., Mulcahy, M.F., Barja, J.L., Culloty, S.C., Romalde, J.L., 2007. The susceptibility of Irish-grown and Galician-grown Manila clams, *Ruditapes philippinarum*, to *Vibrio tapetis* and Brown Ring Disease. J. Invertebr. Pathol. 95, 1–8.

Flye-Sainte-Marie, J., Jean, F., Paillard, C., Ford, S., Powell, E., Hofmann, E., Klinck, J., 2007a. Ecophysiological dynamic model of individual growth of *Ruditapes philippinarum*. Aquaculture 266, 130–143.

Flye-Sainte-Marie, J., Pouvreau, S., Paillard, C., Jean, F., 2007b. Impact of Brown Ring Disease on the energy budget of the Manila clam *Ruditapes philippinarum*. J. Exp. Mar. Biol. Ecol. 349, 378–389.

Flye-Sainte-Marie, J., Jean, F., Paillard, C., Kooijman, S., 2009a. A quantitative estimation of the energetic cost of brown ring disease in the Manila clam using Dynamic Energy Budget theory. J. Sea Res. 62, 114–123.

Flye-Sainte-Marie, J., Soudant, P., Lambert, C., Le Goic, N., Goncalvez, M., Travers, M.A., Paillard, C., Jean, F., 2009b. Variability of the hemocyte parameters of *Ruditapes philippinarum* in the field during an annual cycle. J. Exp. Mar. Biol. Ecol. 377, 1–11.

Ford, S.E., 1986. Effect of repeated hemolymph sampling on growth, mortality, hemolymph protein, and parasitism of oysters, *Crassostrea virginica*. Comp. Biochem. Physiol. 85A, 465–470.

Ford, S., Paillard, C., 2007. Repeated sampling of individual bivalve mollusks I: results and consequences for hemolymph constituents. Fish Shellfish Immunol. 23, 280–291.

Ford, S., Powell, E., Klinck, J., Hofmann, E., 1999. Modeling the MSX parasite in eastern oyster (*Crassostrea virginica*) populations. I. Model development, implementation, and verification. J. Shellfish Res. 18, 475–500.

Goulletquer, P., 1989. Etude des facteurs environnnmentaux intervenant sur la production de la palourde japonaise d'elevage *Ruditapes philippinarum*. Université de Brest Occidentale, Brest, France p. 341.

Goulletquer, P., 1997. A bibliography of the Manila clam *Tapes philippinarum*. In: IFREMER (Ed.), RIDRV-97.02/RA, p. 122 (La Tremblade, France).

Goulletquer, P., Héral, M., Deslous-Paoli, J.-M., Prou, J., Garnier, J., Razet, D., Boromthanarat, W., 1989. Ecophysiology and energy balance of the Japanese clam *Ruditapes philippinarum*. J. Exp. Mar. Biol. Ecol. 132, 85–108.

Heesterbeek, J.A.P., Roberts, M.G., 1995. Mathematical models for microparasites of wildlife. In: Grenfell, B.T., Dobson, A.P. (Eds.), Ecology of Infectious Diseases in Natural Populations. Cambridge University Press, Cambridge, pp. 90–122.

Hoenig, J.M., 1983. Empirical use of longevity data to estimate mortality rates. Fish. Bull. 82, 898–903.

Hofmann, E.E., Powell, E.N., Klinck, J.M., Saunders, G., 1995. Modelling diseased oyster populations I. Modelling *Perkinsus marinus* infections in oysters. J. Shellfish Res. 14, 121–151.

Hofmann, E.E., Klinck, J.M., Kraeuter, J.N., Powell, E.N., Grizzle, R., Buckner, S., Bricelj, V.M., 2006a. A population dynamics model of the hard clam, *Mercenaria mercenaria*: development of the age- and length-frequency structure of the population. J. Shellfish Res. 25, 417–444.

Hofmann, E.E., Klinck, J.M., Kraeuter, J.N., Powell, E.N., Grizzle, R.E., Buckner, S.C., Bricelj, V.M., 2006b. Population dynamics model of the hard clam, *Mercenaria mercenaria*: development of the age- and length-frequency structure of the population. J. Shellfish Res. 25, 417–444.

Jean, F., Flye-Sainte-Marie, J., Oudard, C., Paillard, C., 2011. Handling enhances the development of signs of Brown Ring Disease in *Ruditapes philippinarum*. J. Shellfish Res. 30, 13–15.

Kermack, W.O., McKendrick, A.G., 1991a. Contributions to the mathematical theory of epidemics—I. Bull. Math. Biol. 53, 33–55.

Kermack, W.O., McKendrick, A.G., 1991b. Contributions to the mathematical theory of epidemics—II. the problems of epidemicity. Bull. Math. Biol. 53, 57–87.

Laruelle, F., 1999. Phénologie et déterminisme de la reproduction chez *Ruditapes decussatus* et *R. philippinarum* (Adams et Reeve) en Bretagne, Océanographie Biologique. Université de Bretagne Occidental, Brest p. 230.

Maes, P., 1992. Pathologie bactérienne chez deux invertébres marins d'intérêt commercial, *Ruditapes philippinarum* et *Paracentrotus lividus*. Université de Bretagne Occidentale, Brest p. 217.

Malham, S.K., Coulson, C.L., Runham, N.W., 1998. Effects of repeated sampling on the haemocytes and haemolymph of *Eledone cirrhosa* (Lam.). Comp. Biochem. Physiol. A Mol. Integr. Physiol. 121, 431–440.

McCallum, H., Scott, M.E., 1994. Quantifying population processes: experimental and theoretical approaches. In: Scott, M.E., Smith, G. (Eds.), Parasitic and Infectious Diseases: Epidemiology and Ecology. Academic Press, New York, pp. 29–45.

Monroe, D., Klinck, J., Hoffman, E., Powell, E., 2012. The role of larval dispersal in metapopulation gene flow: local population dynamics matter. J. Mar. Res. 70, 441–467.

Mouritsen, K.N., Tompkins, D.M., Poulin, R., 2005. Climate warming may cause a parasite-induced collapse in coastal amphipod populations. Oecologia 146, 476–483.

Nöel, D., Nicolas, J.-L., Boulo, V., Mialhe, E., Roch, P., 1996. Development of a colony-blot ELISA assay using monoclonal antibodies to identify *Vibrio* P1 responsible for "brown ring disease" in the clam *Tapes philippinarum*. Aquaculture 146, 171–178.

Oubella, R., Maes, P., Paillard, C., Auffret, M., 1993. Experimentally induced variation in hemocyte density for *Ruditapes philippinarum* and *R. decussatus* (Mollusca, Bivalvia). Dis. Aquat. Org. 15, 193–197.

Paillard, C., 1992. Etiologie et Caractérisation de la Maladie de l'Anneau Brun Chez la Palourde d'Elevage, *Ruditapes philippinarum*. Université de Bretagne Occidentale, Brest (pp. Vol I, 194 pp & Vol II, 100 pp.).

Paillard, C., 2004a. Role de l'Environnement dans les Interactions Hôtes — Pathogènes: Développement d'un Modele de Vibriose Chez les Bivalves. Institut Universitaire Européen de la Mer. Université de Bretagne Occidentale, Brest p. 149.

Paillard, C., 2004b. A short review of brown ring disease, a vibriosis affecting clams, *Ruditapes philippinarum* and *Ruditapes decussatus*. Aquat. Living Resour. 17, 467–475.

Paillard, C., Maes, P., 1994. The brown ring disease symptom in the manila clam, *Ruditapes philippinarum*: establishment of a classification system. Dis. Aquat. Org. 19, 137–146.

Paillard, C., Maes, P., 1995a. The Brown Ring Disease in the Manila clam, *Ruditapes philippinarum*. I. Ultrastructural alterations of the periostracal lamina. J. Invertebr. Pathol. 65, 91–100.

Paillard, C., Maes, P., 1995b. The Brown Ring Disease in the Manila clam, *Ruditapes philippinarum*. II. Microscopic study of the brown ring syndrome. J. Invertebr. Pathol. 65, 101–110.

Paillard, C., Maes, P., Oubella, R., 1994. Brown Ring Disease in clams. Ann. Rev. Fish Dis. 4, 219–240.

Paillard, C., Maes, P., Mazurié, J., Claude, S., Marhic, A., Le Pennec, M., 1997. Epidemiological survey of the brown ring disease in clams of Atlantic coast: role of temperature in variation of prevalence. Eighth Symposium of the International Society for Veterinary Epidemiology and Economics. (ISVEE '97). AEEMA Publications, Paris, July 8–11. Paris, France, pp. 14.03.11–14.03.13.

Paillard, C., Allam, B., Oubella, R., 2004. Effect of temperature on defense parameters in Manila clam *Ruditapes philippinarum* challenged with *Vibrio tapetis*. Dis. Aquat. Org. 59, 249–262.

Paillard, C., Kjornes, K., Le Chevalier, P., Le Boulay, C., Harkestad, L., Eriksen, A.G., Willassen, E., Bergh, O., Bovo, C., Skar, C., Mortensen, S., 2008. Isolation of a *Vibrio tapetis*-like strain from introduced Manila clams, *Ruditapes philippinarum*, affected by Brown Ring Disease in Norway. Dis. Aquat. Org. 81 (2), 153–161.

Paraso, M.C., Ford, S.E., Powell, E.N., Hofmann, E.E., Klinck, J.M., 1999. Modeling the MSX parasite in eastern oyster (*Crassostrea virginica*) populations. II. Salinity effects. J. Shellfish Res. 18, 501–516.

Plana, S., Le Pennec, M., 1991. Altérations de la glande digestive et conséquences nutritionelles chez la palourde *Ruditapes philippinarum* contaminée par une bactérie du genre *Vibrio*. Aquat. Living Resour. 4, 255–264.

Plana, S., Sinquin, G., Maes, P., Paillard, C., Le Pennec, M., 1996. Variations in the biochemical composition of the juveniles of manila clam, *Ruditapes philippinarum*, infected by a *Vibrio* sp. Dis. Aquat. Org. 24, 205–213.

Powell, E.N., Hofmann, E.E., Klinck, J.M., Ray, S.M., 1992. Modeling oyster populations I. A commentary on filtration rate. Is faster always better? J. Shellfish Res. 11, 387–398.

Powell, E.N., Klinck, J.M., Hofmann, E.E., Ray, S.M., 1994. Modeling oyster populations IV. Rates of mortality, population crashes, and management. Fish. Bull. 92, 347–373.

Powell, E.N., Hofmann, E.E., Klinck, J.M., 1996. Modeling diseased oyster populations II. Triggering mechanisms for *Perkinsus marinus* epizootics. J. Shellfish Res. 15, 141–165.

Powell, E.N., Klinck, J.M., Hofmann, E.E., Ford, S.E., 1997. Varying the timing of oyster transplant: implications for management from simulation studies. Fish. Oceanogr. 6, 213–237.

Powell, E.N., Klinck, J.M., Ford, S.E., Hofmann, E.E., Jordan, S.J., 1999. Modeling the MSX parasite in eastern oyster (*Crassostrea virginica*) populations. III. Regional application and the problem of transmission. J. Shellfish Res. 18, 517–537.

Powell, E.N., Klinck, J.M., Guo, X., Hofmann, E.E., Ford, S.E., Bushek, D., 2011a. Can oysters develop resistance to Dermo disease in the field: evaluation using a gene-based population dynamics model. J. Shellfish Res. 30, 685–712.

Powell, E.N., Klinck, J.M., Hofmann, E.E., 2011b. Generation time and the stability of sex-determining alleles in oyster populations as deduced using a gene-based population dynamics mode. J. Theor. Biol. 271, 27–43.

Reid, H.I., Soudant, P., Lambert, C., Paillard, C., Birkbeck, T.H., 2003. Salinity effects on immune parameters of *Ruditapes philippinarum* challenged with *Vibrio tapetis*. Dis. Aquat. Org. 56, 249–258.

Riisgard, H.U., 2001. On measurement of filtration rates in bivalves — the stony road to reliable data: review and interpretation. Mar. Ecol. Prog. Ser. 211, 275–291.

Roberts, M.G., Smith, G., Grenfell, B.T., 1995. Mathematical models for macroparasites of wildlife. In: Grenfell, B.T., Dobson, A.P. (Eds.), Ecology of Infectious Diseases in Natural Populations. Cambridge University Press, Cambridge, pp. 177–208.

Soniat, T.M., Brody, M.S., 1988. Field validation of a habitat suitability index model for the American oyster. Estuaries 11, 87–95.

Soniat, T.M., Powell, E.N., Hofmann, E.E., Klinck, J.M., 1999. Understanding the success and failure of oyster populations: the importance of sampled variables and sample timing. J. Shellfish Res. 17, 1149–1165.

Soudant, P., Paillard, C., Choquet, G., Lambert, C., Reid, H.I., Marhic, A., Donaghy, L., Birkbeck, T.H., 2004. Impact of season and rearing site on the physiological and immunological parameters of the Manila clam *Venerupis* (=*Tapes*, =*Ruditapes*) *philippinarum*. Aquaculture 229, 401–418.

Studer, A., Poulin, R., Tompkins, D.M., 2013. Local effects of a global problem: modelling the risk of parasite induced mortality in an intertidal trematode–amphipod system. Oecologia 172, 1213–1222.

Trinkler, N., Labonne, M., Marin, F., Jolivet, A., Bohn, M., Poulain, C., Bardeau, J.F., Paillard, C., 2010a. Clam shell repair from the brown ring disease: a study of the organic matrix using Confocal Raman micro-spectrometry and WDS microprobe. Anal. Bioanal. Chem. 396, 555–567.

Trinkler, N., Sinquin, G., Querne, J., Paillard, C., 2010b. Resistance to Brown Ring Disease in the Manila clam, *Ruditapes philippinarum*: a study of selected stocks showing a recovery process by shell repair. J. Invertebr. Pathol. 104, 8–16.

Trinkler, N., Bardeau, J.F., Marin, F., Labonne, M., Jolivet, A., Crassous, P., Paillard, C., 2011a. Mineral phase in shell repair of Manila clam *Venerupis philippinarum* affected by brown ring disease. Dis. Aquat. Org. 93, 149–162.

Trinkler, N., Guichard, N., Labonne, M., Plasseraud, L., Paillard, C., Marin, F., 2011b. Variability of the shell repair in the Manila clam *Ruditapes philippinarum* affected by the Brown Ring Disease: a study on the organic shell matrix. J. Invertebr. Pathol. 106, 407–417.

White, M.E., Powell, E.N., Ray, S.M., Wilson, E.A., Zastrow, C.E., 1988. Metabolic changes induced in oysters (*Crassostrea virginica*) by the parasitism of *Boonea impressa* (Gastropoda: Pyramidellidae). Comp. Biochem. Physiol. 90 A, 279–290.